Title: HCN1 channels mediate mu opioid receptor long-term depression at insular cortex inputs to the dorsal striatum

Running title: HCN1 mediates opioid LTD in striatum

Braulio Munoz[1], Brandon M. Fritz[1], Fuqin Yin[1], and Brady K. Atwood[1,2].

[1]Department of Pharmacology & Toxicology, Indiana University School of Medicine, Indianapolis, IN, 46202, USA.

[2]Stark Neurosciences Research Institute, Indiana University School of Medicine, Indianapolis, IN, 46202, USA.

Author Contact information

Corresponding author: Brady K. Atwood, PhD.

Indiana University School of Medicine

Department of Pharmacology & Toxicology

320 W 15th St.

NB 400C

Indianapolis, IN, USA 46202

Tel: 317-274-8917

Fax: 317-274-7714

Email: bkatwood@iu.edu

20 **Key Points**

21 - Mu opioid receptor-mediated long-term depression at anterior insular cortex inputs
22 to dorsolateral striatum involves presynaptic cAMP/PKA signaling and protein
23 translation, similar to known mechanisms of endocannabinoid long-term
24 depression.
25 - Dorsal striatal endocannabinoid long-term depression requires mTOR signaling,
26 similar to hippocampal endocannabinoid long-term depression. However, dorsal
27 striatal mu opioid long-term depression does not require mTOR signaling.
28 - Mu opioid long-term depression requires presynaptic HCN1 channels at anterior
29 insular cortex inputs to dorsolateral striatum.

30

Abstract

Mu opioid receptors (MORs) are expressed in the dorsal striatum, a brain region that mediates goal-directed (via the dorsomedial striatum), and habitual (via the dorsolateral striatum, DLS) behaviors. Our previous work indicates that glutamate transmission is depressed when MORs are activated in the dorsal striatum, inducing MOR-mediated long-term synaptic depression (MOR-LTD) or short-term depression (MOR-STD), depending on the input. In the DLS, MOR-LTD is produced by MORs on anterior insular cortex (AIC) inputs and MOR-STD occurs at thalamic inputs, suggesting input-specific MOR plasticity mechanisms. Here, we evaluated the mechanisms of induction of MOR-LTD and MOR-STD in the DLS using pharmacology and optogenetics combined with patch clamp electrophysiology. We found that cAMP/PKA signaling and protein synthesis are necessary for MOR-LTD expression, similar to previous studies of endocannabinoid-mediated LTD (eCB-LTD) in DLS. However, MOR-LTD does not require mTOR signaling as eCB-LTD does. MOR-STD does not utilize these same mechanisms. We characterized the role of presynaptic HCN1 channels in MOR-LTD induction as HCN1 channels expressed in AIC are necessary for MOR-LTD expression in the DLS. These results suggest a mechanism in which MOR activation needs HCN1 to induce MOR-LTD, suggesting a new target for pharmacological modulation of synaptic plasticity, providing new opportunities to develop novel drugs to treat alcohol and opioid use disorders.

Introduction

The opioid system is expressed throughout the brain(Le Merrer *et al.*, 2009) and promotes synaptic plasticity in many brain regions(Bao *et al.*, 2007; Drake *et al.*, 2007; Iremonger & Bains, 2009; Dacher & Nugent, 2011b, a), including the dorsal striatum (DS)(Lovinger, 2010; Atwood *et al.*, 2014a; Hawes *et al.*, 2017; Munoz *et al.*, 2018; Muñoz *et al.*, 2020). The DS is the primary input nucleus of the basal ganglia and can be subdivided in two structures: the dorsomedial striatum (DMS), which controls goal-directed learning, and the dorsolateral striatum (DLS), which regulates habit formation(Hilário & Costa, 2008; Lovinger, 2010; O'Tousa & Grahame, 2014; Burton *et al.*, 2015; Corbit & Janak, 2016). Drug and alcohol use shift from being outcome-driven to becoming more stimulus-driven and compulsive in nature during addiction development(Hopf & Lesscher, 2014; Corbit & Janak, 2016; Everitt & Robbins, 2016; Shen *et al.*, 2018). This transition from flexible goal-directed drug use to more habitual or compulsive use, is paralleled by a transition in the neural activity from the DMS to the DLS(Corbit & Janak, 2016; Shen *et al.*, 2018; Renteria *et al.*, 2020), thereby shifting the balance of action control from DMS to DLS. Previous reports have demonstrated the role of glutamatergic synaptic plasticity in behavior, showing that the disruption of glutamatergic long-term synaptic depression (LTD) at orbitofrontal cortex-DMS synapses prevents habit learning(Gremel *et al.*, 2016), and the disruption of glutamatergic LTD in DLS promotes habit learning(Nazzaro *et al.*, 2012; DePoy *et al.*, 2013). Therefore, changes in the expression of excitatory synaptic plasticity affect specific DS-related behaviors.

Our previous work established that mu opioid receptor (MOR) activation induces long-term synaptic depression (MOR-LTD) or short-term depression (MOR-STD) of glutamate

74 release in both the DLS and DMS(Atwood *et al.*, 2014a; Munoz *et al.*, 2018; Muñoz *et al.*,
75 2020). We demonstrated that MOR-mediated synaptic inhibition is expressed at multiple
76 DS synapses (cortical, thalamic, amygdala and cholinergic), but only a subset of
77 corticostriatal synapses expressed MOR-LTD(Atwood *et al.*, 2014a) that was disrupted
78 by prior *in vivo* ethanol exposure(Munoz *et al.*, 2018; Muñoz *et al.*, 2020). We also found
79 that mice that were exposed to alcohol and the opioid oxycodone *in vivo* had ablated
80 corticostriatal MOR-LTD when measured in brain slices(Atwood *et al.*, 2014a; Munoz *et*
81 *al.*, 2018; Muñoz *et al.*, 2020) MOR plasticity at other DS synapses was unaffected by
82 alcohol exposure(Munoz *et al.*, 2018; Muñoz *et al.*, 2020). Of particular interest, in DLS,
83 alcohol and opioid-sensitive MOR-LTD of glutamatergic input is completely restricted to
84 anterior insular cortex (AIC) inputs(Atwood *et al.*, 2014a; Munoz *et al.*, 2018). Altogether,
85 these data led us to hypothesize that MOR plasticity utilizes different mechanisms at
86 distinct glutamatergic synapses in DS. As we previously demonstrated that MOR-LTD
87 and endocannabinoid LTD (eCB-LTD) are mutually occlusive in DS(Atwood *et al.*, 2014a),
88 we predicted that these two forms of LTD would utilize similar mechanisms. cAMP/PKA
89 signaling mediates eCB-LTD in the nucleus accumbens, amygdala, cerebellum, and
90 hippocampus(Atwood *et al.*, 2014b). In addition, local protein translation in the
91 presynaptic region is enhanced by the activation of CB1 receptor, which is important for
92 the induction of inhibitory LTD in the hippocampus(Younts *et al.*, 2016) and likely also in
93 the DS(Yin *et al.*, 2006). eCB-LTD at GABAergic synapses in the hippocampus is also
94 mediated by mTOR signaling(Younts *et al.*, 2016). Therefore, we sought to test whether
95 MOR-LTD in DLS, and specifically at AIC-DLS synapses is mediated by cAMP/PKA,
96 protein translation and mammalian target of rampamycin (mTOR) signaling. As cAMP

97 also regulates hyperpolarization-activated cyclic nucleotide-gated (HCN) channels, these
98 channels can presynaptically regulate glutamate release, and the type 1 HCN (HCN1)
99 channel may be localized to corticostriatal neurons, we also explored a potential role for
100 HCN1 in mediating MOR-LTD in DLS(Moosmang *et al.*, 1999; Postea & Biel, 2011; He *et*
101 *al.*, 2014; Huang *et al.*, 2017)

102 In the current study, we probed glutamatergic synapses in the DLS using *ex vivo* mouse
103 brain slice electrophysiology. We used broad electrical stimulation in C57BL/6J mice to
104 test all glutamatergic inputs. We used an optogenetics approach to probe specific
105 glutamate synapses in DLS, using Emx1-Ai32 mice to test all cortical inputs, VGluT2-Ai32
106 mice to test all thalamic inputs, and C57BL/6J mice stereotaxically injected with an AAV-
107 ChR2 vector into the AIC to specifically probe AIC-DLS synapses. In combination with
108 these tools, we pharmacologically and genetically probed the mechanism involved in the
109 expression of MOR-LTD in the DLS. We demonstrate that cAMP/PKA signaling and
110 protein synthesis are necessary for MOR-LTD expression, but not for MOR-STD. We
111 describe a novel role of presynaptic AIC HCN1 channels in the induction of MOR-LTD in
112 DLS. We also report that mTOR signaling is required for eCB-LTD of glutamate
113 transmission in the DLS, but this is not required for MOR-LTD indicating a divergence in
114 the mechanisms of these two similar forms of synaptic plasticity.

115

116 **Methods**

117 **Ethical Approval**

118 Animal care and experimental protocols for this study were approved by the Institutional
119 Animal Care and Use Committee (IACUC) at the Indiana University School of Medicine
120 and all guidelines for ethical protocols and care of experimental animals established by
121 the NIH (National Institutes of Health, Maryland, USA) were followed.

122 **Methods details**

123 All experiments were performed similar to our previous dorsal striatal electrophysiological
124 studies with some experiment-specific modifications(Atwood *et al.*, 2014a; Fritz *et al.*,
125 2018; Munoz *et al.*, 2018; Fritz *et al.*, 2019). These methods are described in brief below.

126 **Animals and materials**

127 Male C57BL/6J mice were obtained from the Jackson Laboratory (JAX #000664, Bar
128 Harbor, Maine, USA). Emx1Cre-Ai32, VGluT2Cre-Ai32, and HCN1-flox mice were bred
129 and genotyped in-house (Original stock strains: Ai32: JAX #012569; Emx1Cre: JAX
130 #005628; VGluT2Cre: JAX #016963; HCN1f/f: JAX #028299). All mutant mice used in
131 these studies were backcrossed to C57BL/6J mice for a minimum of 7 generations. The
132 mice used in these studies were between PND 60-100 at the time of experimentation (with
133 the exception of HCN1-flox AAV-cre-injected mice ~PND 98-154). Animals were group-
134 housed in a standard 12-h light/dark cycle (lights on at 0800) at 50% humidity. Food and
135 water were available *ad libitum*.

136 **Reagents**

137 We used the MOR agonist [D-Ala^2, NMe-Phe^4, Gly-ol^5]-enkephalin (DAMGO; H-2535,
138 Bachem), $GABA_A$ receptor antagonist picrotoxin (PTX, P1675, Sigma-Aldrich), PKI (6221,
139 Tocris), KT5720 (1288, Tocris), Forskolin (F3917, Sigma-Aldrich), Cycloheximide (0970,
140 Tocris), ZD7288 (1000, Tocris), WIN55,212-2 (1038, Tocris), and Torin 2 (4248, Tocris).
141 Other reagents used for making solutions were purchased from Sigma-Aldrich or Fisher
142 Scientific.

143 **Brain slice preparation**.

144 Mice were euthanized via decapitation under deep isoflurane anesthesia, and the brain
145 was quickly excised and placed in an ice-cold cutting solution containing (in mM): 194
146 sucrose, 30 NaCl, 4.5 KCl, 1 $MgCl_2$, 26 $NaHCO_3$, 1.2 NaH_2PO_4, 10 Glucose saturated with
147 a mixture of 95% O_2 and 5% CO_2, and sliced to a thickness of 280 µm on a vibratome
148 (Leica VT1200S, Germany). Slices were transferred to an artificial cerebrospinal fluid
149 (aCSF) solution containing (in mM): 124 NaCl, 4.5 KCl, 1 $MgCl_2$, 26 $NaHCO_3$, 1.2
150 NaH_2PO_4, 10 Glucose, 2 $CaCl_2$ (310-320 mOsm) saturated with 95% O_2/5% CO_2 at 30°C
151 for 1 hr before being moved to room temperature. When ready for recording, slices were
152 transferred to a recording chamber continuously perfused with aCSF solution saturated
153 with 95% O_2/5% CO_2.

154 **Electrophysiology recordings**

155 Whole-cell recordings of excitatory postsynaptic currents (EPSCs) in medium spiny
156 neurons (MSNs) were carried out at 29–32 C° and aCSF was continuously perfused at a
157 rate of 1-2 ml/min. Recordings were performed in the voltage clamp configuration using a
158 Multiclamp 700B amplifier and a Digidata 1550B (Molecular Devices, San Jose, CA).

159 Slices were visualized on an Olympus BX51WI microscope (Olympus Corporation of
160 America). MSNs were identified by their size, membrane resistance, and capacitance.
161 Picrotoxin (50 μM) was added to the aCSF for recordings to isolate excitatory transmission.
162 Patch pipettes were prepared from filament-containing borosilicate micropipettes (World
163 Precision Instruments) using a P-1000 micropipette puller (Sutter Instruments, Novato,
164 CA), having a 2.0-3.5 MΩ resistance. The internal solution contained (in mM): 120
165 $CsMeSO_3$, 5 NaCl, 10 TEA-Cl, 10 HEPES, 5 lidocaine bromide, 1.1 EGTA, 0.3 Na-GTP
166 and 4 Mg-ATP (pH 7.2 and 290-310 mOsm). MSNs were voltage clamped at -60 mV for
167 the duration of the recordings. For electrically-evoked recordings, a twisted tungsten
168 bipolar stimulating electrode (PlasticsONE, Roanoke, VA) was placed at the border of the
169 white matter of the external capsule. Electrically-evoked excitatory postsynaptic currents
170 (eEPSCs) were generated by a DS3 Isolated Current Stimulator (Digitimer, Ft. Lauderdale,
171 FL) every 20 s and stimulus intensity was adjusted to produce stable eEPSCs of 200–600
172 pA in amplitude prior to the initiation of experimental recording. To induce eCB1-LTD, high-
173 frequency stimulation (HFS; 4 pulses of 100 Hz, 10 s inter-pulse interval) coupled with
174 depolarization (0 mV) was delivered after 10 minutes of baseline recording(Atwood *et al.*,
175 2014a; Munoz *et al.*, 2018). To induce hippocampal LTP, the internal solution contained
176 (in mM): 126 K-gluconate, 4 KCl, 10 phosphocreatine, 10 HEPES, 0.3 Na-GTP and 4 Mg-
177 ATP (pH 7.2 and 290-310 mOsm) and the MSNs were held at -80mV. After the baseline
178 was established, LTP was induced by switching the mode to current-clamp and delivering
179 high-frequency stimulation (HFS; 4 pulses of 100 Hz, 1 min inter-pulse interval) as
180 previously reported(Duffy & Nguyen, 2003). The spontaneous EPSC (sEPSC) recordings
181 were made for 2 min and the analysis of frequency (Hz), decay constant (ms), rise constant

182 (ms) and amplitude (pA) were measured to determine the effects of the blockade of striatal
183 HCNs and the deletion of HCN1 in AIC. The decay constant of sEPSCs was fitted as single
184 exponential and both rise and decay-phase were fitted between 10 and 90% of the maximal
185 amplitude. Data were acquired using Clampex 10.3 (Molecular Devices, San Jose, CA).
186 Series resistance was monitored and only cells with a stable series resistance (less than
187 25 MΩ and that did not change more than 15% during recording) were included for data
188 analysis. Recordings were made 2–7 h after euthanasia.

189 **Viral injections**

190 C57BL/6J mice were anesthetized with isoflurane and stereotaxically-injected with the
191 adeno-associated viral (AAV) vector, AAV9.hSyn.ChR2(H134R)-eYFP (Addgene #26973)
192 to drive ChR2 expression in AIC neurons. Bilateral injections were made into AIC: A/P:
193 +2.4, M/L: ±2.3, D/V: −2.25 (50 nl/injection, 12.5 nl/min infusion rate).

194 To produce AIC projection neuron HCN1 knockout mice, HCN1-flox mice were
195 anesthetized with isoflurane and stereotaxically-injected with
196 AAV9.hSyn.HI.eGFP.Cre.WPRE.SV40 (Addgene #105540) or
197 AAV9.hSyn.eGFP.WPRE.bGH as control (Addgene #105539). Bilateral injections were
198 made into AIC at coordinates: A/P: +2.4, M/L: ±2.3, D/V: −2.25 (75 nl/injection, 12.5 nl/min
199 infusion rate). HCN1-flox mice were allowed to recover for at least 4 weeks to allow for
200 adequate ablation of HCN1 channel expression before brain slices were made for
201 electrophysiological recordings. Prior to recording, brain slices were imaged via an
202 Olympus MVX10 microscope (Olympus Corporation of America) to verify GFP or GFP-
203 tagged cre-recombinase expression in injected HCN1-flox mice.

204 **Optogenetic Recordings**

205 AAV-ChR2 injection in C57BL/6J mice was performed to target ChR2 expression to inputs
206 from AIC to DLS. Optically-evoked EPSCs (oEPSCs) in MSNs from Emx1-Ai32, VGluT2-
207 Ai32 and C57BL/6J mice injected with AAV-ChR2 were produced in brain slices using 470-
208 nm blue light (5-ms exposure time) delivered via field illumination through the microscope
209 objective. Light intensity was adjusted to produce stable oEPSCs of 200–600-pA amplitude
210 prior to experimental recording. oEPSCs were evoked every 30s. AIC-DLS eCB-LTD was
211 produced using optical high-frequency stimulation (oHFS) coupled with depolarization (4
212 blue light pulses of 50 Hz, 10 s inter-pulse interval). Prior to recording, brain slices were
213 imaged via an Olympus MVX10 microscope (Olympus Corporation of America) to verify
214 YFP-tagged ChR2, GFP-tagged cre-recombinase, or GFP expression in injected
215 C57BL/6J mice. Injection site location were determined from matching images to the
216 Reference Allen Mouse Brain Atlas (Figs. 2 and 12). Animals that did not have viral
217 expression in the AIC were excluded from the study

218 **Quantitative polymerase chain reaction**

219 Anterior insular cortex tissues were taken from HCN1-flox/AAV-cre (+) and HCN1-
220 flox/AAV-GFP (−) mice. RNA was isolated from brain tissue using the RNeasy Plus
221 Universal Mini Kit (Qiagen #73404) according to the manufacturer's protocol. Total RNA
222 (50 ng/µl) was converted to complementary DNA (cDNA) using the High Capacity cDNA
223 Reverse Transcription kit (Catalog number: 468814, Applied Biosystems Inc. (ABI), Foster
224 City, CA) and amplified using a CFX Connect real-Time PCR detection System (Bio-Rad
225 Laboratories). The TaqMan probe used in the current study was Hcn1 (PrimePCR™
226 Assay: Hcn1.Mmu, Unique Assay ID:qMmuCED0045731, Catalog #10025636,

227 ThermoFisher). Quantitative PCR was performed using SsoAdvanced Universal Probes
228 Supermix (Catalog #: 172-5280, Bio-Rad Laboratories). The relative amount of each
229 transcript was determined via normalization across all samples to the endogenous control
230 glyceraldehyde 3-phosphate dehydrogenase (GAPDH) (Catalog: Mm.PT.39a.1,
231 PrimeTime Std® qPCR Assay, IDT, IA, USA) to account for variability in the initial
232 concentration and quality of the total RNA and in the conversion efficiency of the reverse
233 transcription reaction as recommended by ABI. In addition, before initiation of the analysis,
234 cDNA was diluted 1:10 and amplified using the respective TaqMan probes to ensure that
235 the amount of cDNA used was in the linear range. RNA samples from each individual
236 animal were run in duplicate.

237 To quantify the relative expression levels of the different genes for each mouse genotype,
238 we calculated the difference (ΔCt) between the cycle threshold of Hcn1 and the
239 housekeeping gene glyceraldehyde 3-phosphate dehydrogenase (GAPDH). From these
240 data, the ΔΔCt ([ΔCt(Cre (+))–ΔCt(GFP (-))]) was computed and converted to a relative
241 quantitative (RQ) value using the formula $2^{-\Delta\Delta Ct}$. The results were tabulated as
242 mean ± SD and compared between genotypes via unpaired Student's t tests.

243 **Quantification and statistical analysis**

244 **Sample size**

245 The target number of samples in each group for electrophysiological experiments was
246 determined from our previously published studies(Atwood *et al.*, 2014a; Munoz *et al.*, 2018;
247 Muñoz *et al.*, 2020).

248 **Replication**

249 Sample sizes indicated in figures for electrophysiological experiments represent biological
250 replicates. Due to the inherent biological variability between neurons recorded
251 (biochemical makeup and innervation patterns), neurons were considered the unit of
252 biological replication. 1 neuron was recorded per brain slice and all experiments involved
253 recordings from at least 3 mice.

254 **Data analyses**

255 eEPSCs and oEPSCs were analyzed using Clampfit 10.1 (Molecular Devices, San Jose,
256 CA) and sEPSCs with MiniAnalysis 6.0 (Synaptosoft Inc). Data are presented as the
257 mean ± SD in the main text and as mean ± SEM (time courses) or as box plots
258 representing medians and interquartile ranges in the figure legends. The analyses of
259 normally distributed data were performed using two-tailed unpaired or two-tailed paired
260 Student's t tests following an F test to confirm similar variances. Non-normally distributed
261 data were analyzed using two-tailed Welch's t test for unpaired data (Fig. 7D). One-way
262 ANOVA following Dunnett's multiple comparisons test was performed to compare controls
263 from treatments in Figs. 4G, N, U and 9M. Repeated measures One-way ANOVA
264 following Tukey's multiple comparisons test was performed for Fig. 9C, F, I and L. Data
265 that were analyzed using this test are indicated in the figure legends. Statistical analyses
266 were performed with Prism 9 (GraphPad, La Jolla, CA). The level of significance was set
267 at $P < 0.05$ for all analyses. Representative traces are the average baseline EPSC (1-10
268 min), average of the acute DAMGO response (12-20 min) and average post-treatment
269 EPSC of final 10 min of recording. Exclusion of individual data points was determined
270 using a ROUT outlier calculator (Q=1%) included in the Prism 9 software package.

271

272 **Results**

273 **MOR activation express glutamatergic LTD in the DLS**

274 We previously showed that the activation of MOR in DLS produces LTD of eEPSCs as
275 well as oEPSCs(Munoz *et al.*, 2018). Using three approaches, we confirmed that 5 min
276 application of the MOR agonist DAMGO (0.3 μM) induces MOR-LTD. We found that
277 DAMGO produced a persistent decrease in eEPSC amplitude in DLS MSNs (74 ± 10%;
278 Fig. 1A-D) in brain slices from C57Bl/6J mice. To generally probe corticostriatal synapses,
279 we used 470 nm light delivered through the microscope objective to evoke oEPSCs in
280 brain slices from Emx1-Ai32 mice (Fig. 1E), where the activation of MOR again induced
281 MOR-LTD (75 ± 10%; Fig. 1F-H). Finally, to specifically stimulate the release of glutamate
282 from AIC inputs to the DLS, we infused an AAV vector expressing ChR2 in the AIC (Fig.
283 1I, Fig. 2), as we previously did(Munoz *et al.*, 2018). As shown previously, activation of
284 MORs produced glutamatergic LTD of AIC-DLS transmission (76 ± 15%; Fig. 1J-L).
285 These data replicate our previous work that MORs mediated LTD of AIC-DLS synapses.
286 We previously showed that eCB-LTD and MOR-LTD were mutually occlusive in
287 DLS(Atwood *et al.*, 2014a). In order to determine whether we could infer potential MOR-
288 LTD mechanisms from what is known about eCB-LTD, we investigated whether eCB-LTD
289 also occurred at AIC-DLS synapses. We used the same AAV approach described above
290 (Fig. 3A) and tested the effects of stimulation-induced LTD and responses to the CB1
291 receptor agonist WIN55,212-2 (1 μM). We found that eCB-LTD (65 ± 7%; Fig. 3B, C, D
292 and F) and CB1 agonist-induced LTD (68 ± 7%; Fig. 3B, C, E and F) both occur at AIC-
293 DLS synapses. Next, we explored the signaling cascades that mediate MOR plasticity in
294 DLS using what is known about eCB-LTD as a guide for our experiments.

295 **Inhibition of presynaptic PKA blocks MOR-mediated LTD**

296 The activation of opioid receptors produces an inhibition of adenylyl cyclase (AC)
297 mediated by Gαi, decreasing cAMP levels, which leads to an attenuation of cAMP/protein
298 kinase A (PKA) signaling(Atwood *et al.*, 2014b; Reeves *et al.*, 2022). However, little is
299 known about PKA's role in MOR-mediated LTD. Using KT5720 (1 μM), a specific and cell
300 permeable inhibitor of PKA, which brain slices were incubated in for 1h prior to recordings,
301 we demonstrated that the inhibition of PKA blocks the maintenance of MOR-LTD of
302 eEPSCs in DLS (101 ± 19%; Fig. 4A-C and G). Corticostriatal MOR-LTD was also blocked
303 by PKA inhibition (94 ± 16%; Fig. 4H-J and N), as was MOR-LTD at AIC-DLS synapses
304 (94 ± 11%; Fig. 4O-Q and U). We found that these effects were due to inhibiting
305 presynaptic PKA activity as at least 30 min treatment with the membrane-impermeable
306 PKA inhibitor PKI (1 μM), intracellularly infused through the recording micropipette into
307 the postsynaptic MSN, did not affect MOR-LTD in the DLS (eEPSCs: 84 ± 7%; Fig. 4D-
308 G) (corticostriatal oEPSCs: 64 ± 20%; Fig. 4K-N) (AIC-DLS oEPSCs: 69 ± 11%; Fig. 4R-
309 U). Since this was a negative effect, we needed to test if PKI was able to induce any
310 effect, therefore, we evaluated PKI in a brain region where the inhibition of postsynaptic
311 PKA disrupts synaptic plasticity(Duffy & Nguyen, 2003). We found that intracellular PKI
312 application blocked the expression of long-term potentiation (LTP) in hippocampal CA1
313 pyramidal neurons (Control: 151 ± 30% vs PKI: 95 ± 30%, Fig. 5). As we expected, our
314 data demonstrate the role of presynaptic PKA in MOR-LTD.

315 **The activation of adenylyl cyclase disrupts MOR-mediated LTD**

316 Demonstrating a role for PKA signaling in MOR-LTD implicates adenylyl cyclase (AC)
317 signaling as mediating MOR-LTD. To more specifically test this, we persistently activated

318 AC using 20 μM forskolin throughout recording. In the presence of forskolin, DAMGO
319 produced a transient increase of the EPSC amplitudes (Fig. 6A, B, E, F, I and J), followed
320 by a blockade MOR-LTD at all excitatory synapses (105 ± 14%; Fig. 6A-D) and at
321 corticostriatal (105 ± 6%; Fig. 6E-H) and AIC inputs (98 ± 14%; Fig. 6I-L). Altogether,
322 these findings indicate that cAMP/PKA signaling pathway is involved in the induction and
323 maintenance of MOR-LTD in DLS.

324 **Protein translation is required to produce MOR-mediated LTD**

325 Next, we tested the role of protein translation in MOR-LTD. Using, bath application of 80
326 μM cycloheximide (selective inhibitor of protein synthesis) during the entire recording, we
327 found that the inhibition of protein translation blocked MOR-LTD generally (105 ± 33%;
328 Fig. 7A-D) and specifically at cortical (102 ± 18%; Fig. 7E-H) and AIC inputs (94 ± 10%;
329 Fig. 7I-L).

330 It had been reported that eCB protein translation-mediated-LTD involves mTOR signaling
331 in the hippocampus(Younts *et al.*, 2016). To test if mTOR is required for eCB-LTD also in
332 the DLS, we used bath application of 100 nM Torin 2 (a selective mTOR inhibitor). We
333 demonstrated that the inhibition of mTOR signaling disrupted eCB-LTD in the DLS
334 (Control: 76 ± 8% vs Torin 2: 95 ± 5%; Fig. 8A-D). However, MOR-LTD does not require
335 mTOR signaling in the DLS (79 ± 7%; Fig. 8E-H). These data suggest that protein
336 translation is necessary for MOR-mediated LTD, but mTOR signaling is not involved and
337 indicate that eCB- and MOR-LTD, while qualitatively similar, do not utilize identical
338 signaling mechanisms.

339 **MOR-STD from thalamocortical inputs is not affected by PKA inhibition, cAMP**
340 **activation or protein translation inhibition.**

341 We also confirmed that thalamostriatal inputs expressed MOR-STD in the DLS using
342 VGluT2-Ai32 transgenic mice (12-20 min: 68 ± 5%; 30-35 min: 93 ± 7%; Fig. 9A-B and
343 M) as we previously showed(Atwood *et al.*, 2014a; Munoz *et al.*, 2018). These data
344 replicate our previous work that MORs mediated STD of thalamostriatal synapses in the
345 DLS. Unlike corticostriatal inputs, these thalamostriatal inputs, were not affected by broad
346 inhibition of PKA (12-20 min: 81 ± 15%; 30-35 min: 108 ± 26%). Inhibition of postsynaptic
347 PKA had no effect on MOR-STD (12-20 min: 86 ± 9%; 30-35 min: 115 ± 31%; Fig. 9D-F
348 and M), just as it had no effect on MOR-LTD. MOR-mediated STD at thalamic synapses
349 was also not affected by the application of forskolin (12-20 min: 81 ± 13%; 30-35 min: 89
350 ± 15%; Fig. 9G-I and M) or cycloheximide treatment (12-20 min: 76 ± 18%; 30-35 min:
351 101 ± 23%; Fig. 9J-M). Altogether, these data indicate that MOR-STD at thalamic inputs
352 to DLS does not utilize the same mechanisms that MOR-LTD does.

353 **Presynaptic HCN1 channels are indispensable for MOR-mediated LTD**

354 Given that we identified cAMP signaling as important for MOR-LTD expression (Fig. 6),
355 we also explored the possibility of HCN1 channels as key factors for MOR-LTD. To do
356 so, we applied the general HCN blocker ZD7288 (25 μM) to brain slices for at least 30
357 minutes before DAMGO application and during the entire recording. HCN inhibition
358 blocked the expression of MOR-LTD (104 ± 17%; Fig. 10A-D), suggesting a novel role
359 for HCN channels in DLS glutamatergic synaptic plasticity. Next, we characterized the
360 effects of HCN channels in glutamatergic DLS synaptic transmission, by bath applying 25
361 μM ZD7288 for at least 15 minutes before recording sEPSCs. We found that the inhibition

362 of HCN channels caused an enhancement in the frequency and a decrease in the
363 amplitude of sEPSCs (Fig. 10E-G), without affecting rise and decay times (Fig. 10H and
364 I). These data suggest, that HCN channels in the DLS both modulate synaptic
365 transmission and mediate MOR-LTD.

366 To further characterize this new role of HCN channels and specifically establish that
367 presynaptic HCN1 channels are involved in the mechanism of expression of MOR-LTD,
368 we used conditional HCN1 knockout mice (HCN1-flox) injected with AAV-cre vector into
369 AIC to reduce the expression of HCN1 channel specifically in the AIC, and used AAV-
370 GFP vector-infused mice as controls (Fig. 11A, B and Fig. 12). We used qPCR to confirm
371 that AAV-cre infusion reduced HCN1 expression in the AIC (cre: 0.65 ± 0.2 vs GFP: 1.07
372 ± 0.4, Fig. 11C). Next, using electrical stimulation and recording in the DLS, we found that
373 the ablation of HCN1 expression in the AIC reduced the magnitude of MOR-LTD in AAV-
374 cre-injected mice, relative to AAV-GFP-injected mice (cre: 91 ± 12% vs GFP: 77 ± 10%;
375 Fig. 11D-H). Next, we tested if the reduction of presynaptic HCN1 channels produced
376 changes in basal striatal glutamatergic transmission. We found that the decrease of AIC
377 HCN1 channels did not affect any synaptic parameters (Fig. 11I-M). These data suggest
378 that HCN1 channels specifically on AIC inputs are necessary for MOR-LTD expression in
379 the DLS.

380

381 **Discussion**

382 The current study demonstrates that the mechanism of MOR-mediated LTD is similar to
383 the mechanism of induction of the inhibition of glutamate of CB1 or eCB-LTD in that it
384 involves cAMP-PKA-protein translation signaling and both occur at AIC-DLS synapses
385 (Lonart *et al.*, 2003; Yin *et al.*, 2006; Mato *et al.*, 2008; Yasuda *et al.*, 2008; Atwood *et al.*,
386 2014b; Younts *et al.*, 2016). However, we found notable differences such as a lack of
387 dependence on mTOR signaling (Fig. 8) and a novel mechanism involving HCN1
388 signaling for MOR-LTD (Fig. 10 and 11). Figure 13 summarizes the findings of the paper
389 and illustrates the differential mechanisms involved in the expression of MOR-mediated
390 LTD. Furthermore, the MOR-LTD mechanism is different than that of MOR-STD (Fig. 13),
391 suggesting that MOR-mediated plasticity does not utilize a common pathway at all
392 glutamatergic synapses.

393 Our previous report demonstrates that MORs expressed in AIC are the sole source of
394 MOR-mediated LTD at glutamate inputs to the DLS(Munoz *et al.*, 2018). However in the
395 DMS, MORs on medial prefrontal cortex, anterior cingulate cortex, and basolateral
396 amygdala inputs are capable of inducing LTD(Muñoz *et al.*, 2020). MOR-LTD also occurs
397 locally at cholinergic interneuron synapses that co-release glutamate on to MSNs(Munoz
398 *et al.*, 2018; Muñoz *et al.*, 2020). However, alcohol only disrupts MOR-LTD at AIC inputs
399 to DLS and at medial prefrontal and anterior cingulate cortex inputs to DMS leaving MOR
400 plasticity at thalamostriatal, amygdalostriatal and cholinergic interneurons
401 unaffected(Munoz *et al.*, 2018; Muñoz *et al.*, 2020). We also found that the opioid
402 oxycodone disrupts MOR-LTD in DLS(Atwood *et al.*, 2014a), and given that this is
403 mediated by AIC-DLS MORs(Munoz *et al.*, 2018), it follows that alcohol and opioids have

404 similar actions on MOR plasticity at this synapse. Given that alcohol (and presumably
405 oxycodone and other opioids) do not affect MOR plasticity at these other non-
406 corticostriatal synapses, differential mechanisms that underlie MOR plasticity at each type
407 of synapse may confer susceptibility to the deleterious effects of these drugs and could
408 account for their mechanisms of action in the development of habitual or compulsive use
409 of the drugs.

410 Previous work has shown that the inhibition of PKA disrupts eCB-LTD in the nucleus
411 accumbens(Mato *et al.*, 2008) and that presynaptic PKA is required to induce cannabinoid
412 LTD in cerebellum(Lonart *et al.*, 2003) and eCB synaptic plasticity in
413 hippocampus(Yasuda *et al.*, 2008). Moreover, previous reports had shown that the
414 activation of AC by forskolin enhances corticostriatal EPSC amplitudes(Cho *et al.*, 2008)
415 and blocked delta opioid receptor-mediated LTD of inhibitory postsynaptic
416 currents(Patton *et al.*, 2016). cAMP/PKA signaling has also been implicated in
417 presynaptic type 2/3 metabotropic glutamate receptor- and type 1b serotonin receptor-
418 mediated LTD at various synapses in the brain(Atwood *et al.*, 2014a). As previously
419 reported(Duffy & Nguyen, 2003), we confirmed that the activation of postsynaptic PKA is
420 necessary for the induction of LTP in CA1 pyramidal neurons from the hippocampus, but
421 not for MOR-LTD in DLS (Fig. 5). Until now, the role of cAMP/PKA signaling pathway in
422 MOR-mediated plasticity had not been addressed. Our results demonstrate that
423 presynaptic PKA inhibition blocked AIC-DLS MOR-LTD (Fig. 4 and 13), but not
424 thalamostriatal MOR-STD (Fig. 9D-F and 13). Interestingly, the magnitudes and time
425 courses of eEPSCs and oEPSCs did not differ between measures (Fig. 4A, D, H, K, O
426 and R), suggesting that PKA is not required for an acute MOR-mediated inhibition of

427 glutamate release, but it is required for the maintenance of MOR-LTD. On the other hand,
428 we found that AC activation disrupted both acute MOR-mediated inhibition (in fact turning
429 it into a transient potentiation) and MOR-LTD (Fig. 6 and 13), but had no effect on MOR-
430 STD (Fig. 9G-I and M and 13). Altogether these data suggest that cAMP/PKA pathway
431 may be a general mechanism whereby GPCRs that signal through Gαi may induce LTD,
432 but a receptor's ability to couple to Gαi does not necessarily mean that it will induce
433 cAMP/PKA-dependent LTD upon activation.

434 Protein translation is necessary for striatal eCB-LTD(Yin *et al.*, 2006) and is involved in
435 GPCR-mediated LTD at some synapses, but not others(Atwood *et al.*, 2014a; Younts *et*
436 *al.*, 2016) suggesting that protein translation can be an important component of
437 glutamatergic LTD, depending on the synapse. Indeed, local protein translation can take
438 place in the presynaptic region, where the activation of CB1 receptors enhances protein
439 translation, being critical for the induction and not the maintenance of inhibitory
440 LTD(Younts *et al.*, 2016). Here we demonstrated that protein translation is necessary to
441 produce MOR-LTD (Fig. 7 and 13), but not MOR-STD (Figure 9J-M and 13). Our data is
442 consistent with the previous reports on protein translation-dependent eCB-LTD, and
443 suggest that it is presynaptic protein translation that is involved in MOR-LTD expression.
444 However, cycloheximide has been reported to also activate p38/MAPK signaling
445 (Lockhead *et al.*, 2020) and several studies have shown a critical role of p38 kinases in
446 the induction of LTD and LTP (Asih *et al.*, 2020). Therefore, more data is needed to
447 determine this is definitively protein translation-mediated in the DLS.

448 Although we have previously reported that MOR- and eCB-LTD are mutually occlusive in
449 the DLS(Atwood *et al.*, 2014a), and here we found that there were similarities between

450 MOR-LTD and eCB-LTD mechanisms, we found some differences which make both
451 types of LTD distinct. In the DLS, MOR-LTD of glutamate input is restricted to the
452 AIC(Munoz *et al.*, 2018), which differs from the more broadly expressed (and overlapping
453 at AIC-DLS synapses, Fig. 3) eCB-LTD(Wu *et al.*, 2015; Gremel *et al.*, 2016), suggesting
454 that these two forms of LTD may occur in distinct synaptic environments that could utilize
455 differing mechanisms. It is likely that even in synapses where both receptors are
456 expressed (e.g. in AIC terminals) that each receptor shares partially overlapping, but not
457 identical signaling pathways.

458 A clear example of distinct signaling mechanisms identified here is in the role of the mTOR
459 pathway in eCB-LTD and MOR-LTD. The CB1 receptor can signal via mTOR in the
460 hippocampus, where the increase of protein translation induced by CB1 receptor
461 activation is mTOR-dependent producing inhibitory eCB-LTD(Younts *et al.*, 2016). We
462 predicted that we would see the same effect in the DLS for both eCB-LTD and for MOR-
463 LTD. Partially correct in our prediction, we found that eCB-LTD is blocked after the
464 inhibition of mTOR in the DLS (Fig. 8A-D), but the mechanism of MOR-LTD did not utilize
465 mTOR (Fig. 8E-H). These novel data regarding eCB-mTOR signaling in DLS provide
466 rationale for future experiments addressing the role of eCB-mTOR signaling in dorsal
467 striatal- related behaviors.

468 Presynaptic cations such as Na^+ and K^+ are important for the propagation of action
469 potentials and subsequent glutamate release(Chen & Lui, 2021). HCNs channels are
470 permeable to Na^+ and K^+ and modulated by cAMP(Sartiani *et al.*, 2017), and they can
471 decrease neurotransmission by restricting presynaptic Ca^{2+} influx(Huang *et al.*, 2011).
472 However, while we did not find that Ca^{2+} plays a role in MOR-LTD, we did identify a critical

473 role for the HCN1 channel in MOR-LTD expression (Fig. 10, 11 and 13). It has been
474 reported that HCN1 channels can be found at presynaptic sites in the globus pallidus,
475 where the inhibition by ZD7288 produced an increase of miniature inhibitory postsynaptic
476 current frequency, with no changes in amplitude(Boyes *et al.*, 2007). The block or deletion
477 of HCN1 causes an increase in the frequency of miniature EPSCs in entorhinal cortical
478 pyramidal neurons(Huang *et al.*, 2011). Here we showed that broad blockade of HCN
479 channels enhanced glutamate release, but decreased postsynaptic responses to
480 glutamate (Fig. 10E-I), presumably by acting non-specifically at both presynaptic and
481 postsynaptic sites. However, when we deleted just HCN1 from AIC inputs to DLS (Fig.
482 11C), we did not observe any changes in basal glutamate transmission (Fig. 11I-M). The
483 differences in effects of broad blockade and synapse-specific deletion may be attributed
484 to the overall contribution of HCN1s at AIC inputs relative to the population of glutamate
485 synapses. Genetic deletion did not completely ablate MOR-LTD expression (Fig. 11G).
486 This could be due to an incomplete AAV vector transduction (most recordings had a
487 complete loss of LTD) or perhaps that HCN1 contributes to LTD differently at AIC inputs
488 to different subtypes of MSNs. Therefore, in the future, it will also be important to
489 investigate the role of HCN1 in MOR-LTD at AIC inputs to D1- or D2-expressing MSNs
490 (direct or indirect pathway respectively). It has recently been reported that HCN1
491 contributes to alcohol preference(Salling & Harrison, 2020). Given that alcohol disrupts
492 MOR-LTD in DLS, this mechanism of MOR-HCN1 signaling may be a target of alcohol's
493 effects and contribute to alcohol-related, dorsal striatal-dependent behaviors such as
494 habitual and compulsive alcohol drinking. As the opioid oxycodone also disrupts MOR-
495 LTD it will be intriguing to determine the impact of both oxycodone and alcohol on AIC-

496 DLS HCN1 function. HCN1 may therefore have therapeutic potential in alcohol and opioid
497 use disorders.

498 In conclusion, these findings indicate that glutamatergic synapses in the DLS have distinct
499 mechanisms of plasticity induction mediated by the same types of receptors. The specific
500 signaling processes that result in these different forms of plasticity might be the answer
501 to why different types of plasticity are differentially sensitive to drugs of abuse and alcohol
502 (Fig. 13) (Atwood *et al.*, 2014b; Munoz *et al.*, 2018; Muñoz *et al.*, 2020). However, further
503 work is required to resolve what components of these mechanisms render some
504 synapses susceptible to the deleterious effects of these drugs while others are resistant.
505 It will also be important to decipher the behavioral relevance of AIC-DLS synapse HCN1
506 channels and eCB-mTOR signaling in the DLS.

507

508 **Additional Information**

509 **Data availability statement**

510 All data in this study are available upon reasonable request to the corresponding author.
511 All reagents and other materials used for this work are commercially available.

512 **Competing interests**

513 The authors declare no conflict of interest.

514 **Author Contributions**

515 B.M., and B.K.A., designed experiments, discussed the results, contributed to all stages
516 of manuscript preparation and editing. BM performed and analyzed all experiments.
517 B.M.F., assisted in collecting electrophysiological data. F.Y. performed qPCR experiment.
518 All authors contributed to and approved the final version of the manuscript.

519 **Funding**

520 This work was supported by NIH/NIAAA grant R01 AA027214.

521 **Keywords**

522 Synaptic plasticity, long-term depression, Striatum, Opioid, Cannabinoids, mu opioid
523 receptor, insular cortex, HCN1 channel.

524 **Supporting information**

Additional supporting information can be found online in the Supporting Information section at the end of the HTML view of the article. Supporting information files available:

Peer Review History

Statistical Summary Document

530 **Figures**

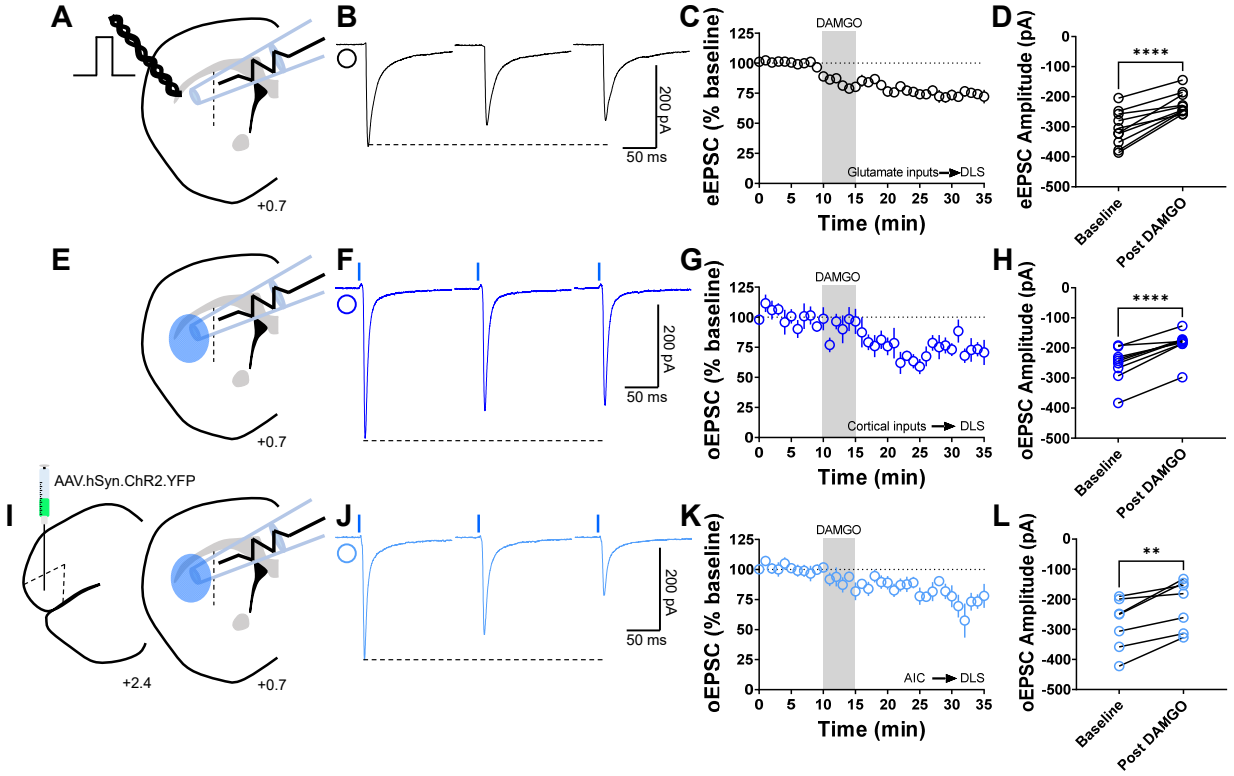

531
532 **Figure 1. MOR activation induces glutamatergic LTD in the DLS. (A)** Schematic
533 representation of coronal brain slice showing the recording of EPSCs evoked by focal
534 electric stimulation in the DLS of C57BL/6J mice. **(B)** Representative electrically-evoked
535 EPSC traces before, during and after DAMGO (0.3 μM, 5 min) application. **(C)** The
536 activation of MOR by DAMGO induced glutamatergic LTD in DLS MSNs of C57BL/6J
537 (final 10 min of recording average: 74 ± 3%). **(D)** eEPSC amplitudes in MSNs within DLS
538 were significantly reduced after DAMGO application (0–10 min baseline v. final 10 min of
539 recording; paired t-test, P=0.00009, t9 =6.688, n = 10 neurons from 5 mice). **(E)**
540 Schematic representation of coronal brain slice showing the recording of EPSCs evoked
541 by focal optical stimulation (470-nm blue light for 5-ms exposure) in the DLS of Emx1-
542 Ai32 mice. **(F)** Representative optically-evoked EPSC traces before, during and after
543 DAMGO (0.3 μM, 5 min) application. **(G)** The activation of MOR by DAMGO induced
544 corticostriatal LTD in DLS MSNs of Emx1-Ai32 (final 10 min of recording average: 75 ±
545 3%). **(H)** oEPSC amplitudes were significantly reduced after DAMGO application (0–
546 10 min baseline v. final 10 min of recording; paired t-test, P=0.00006, t8 =7.73, n = 9
547 neurons from 4 mice). **(I)** Schematic figure of the injection paradigm showing an AAV
548 vector encoding for ChR2 (AAV.hSyn.ChR2.YFP) in AIC in C57BL/6J mice, this AAV was
549 injected 2 weeks prior to recordings. Also, the next schematic representation of coronal
550 brain slice shows the recording of oEPSCs (470-nm blue light for 5-ms exposure) in the
551 DLS. **(J)** Representative AIC-DLS oEPSC traces before, during and after DAMGO
552 (0.3 μM, 5 min) application. **(K)** DAMGO induced AIC-DLS LTD (final 10 min of recording
553 average: 76 ± 5%). **(L)** DAMGO application significantly reduced oEPSC amplitudes (0–

554 10 min baseline v. final 10 min of recording; paired t-test, $P = 0.004$, $t_6 = 4.5$, $n = 7$ neurons
555 from 4 mice). Data represent mean ± SEM. **$P < 0.01$, ****$P < 0.0001$.

556

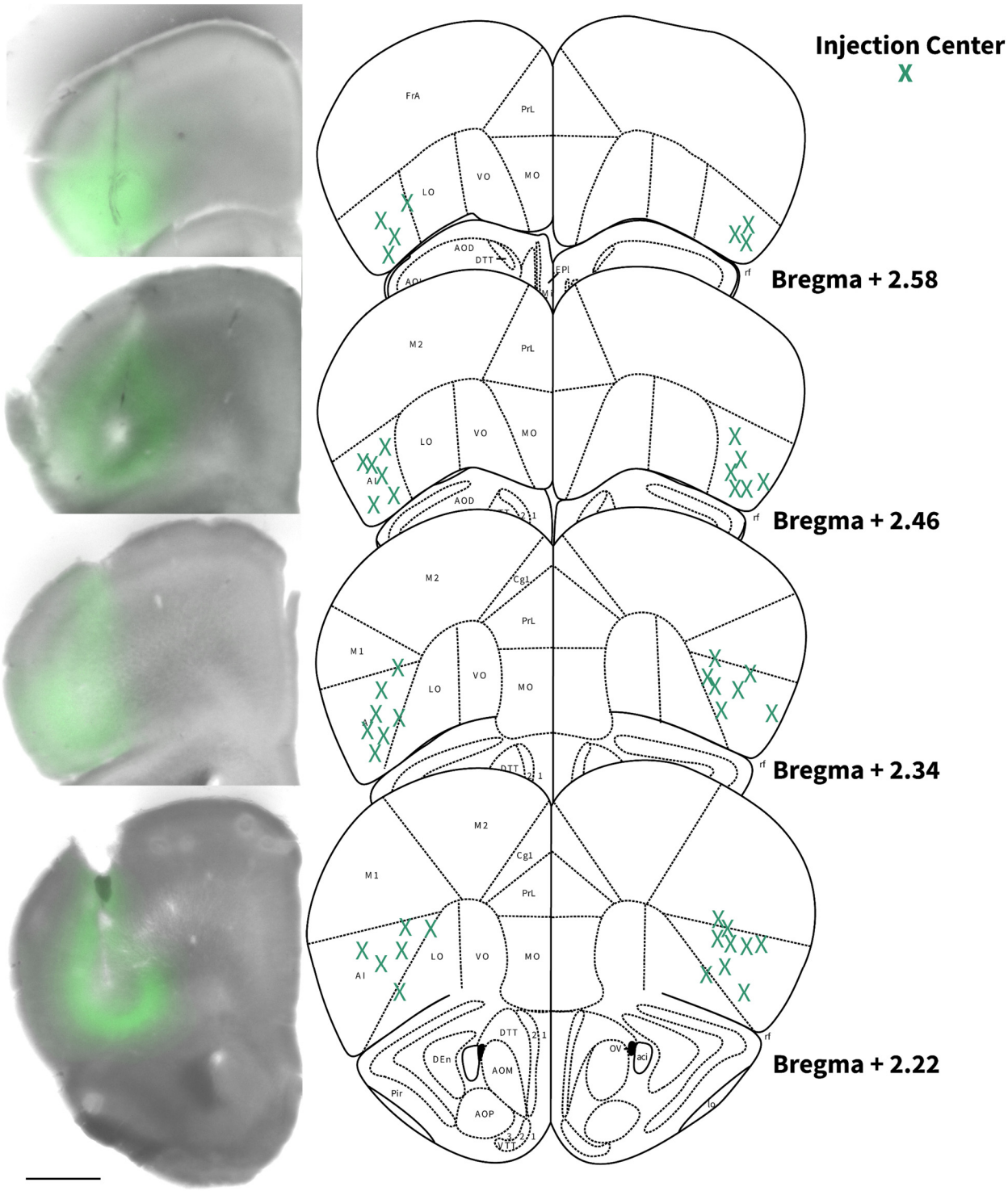

Figure 2. Locations of AIC injections for DLS electrophysiology. Coronal brain hemi slices images and schematic figures modified from Allen Mouse Brain Atlas showing bilateral injection centers of AAV-ChR2-EYFP in the AIC of C57BL/6J mice verified by histology.

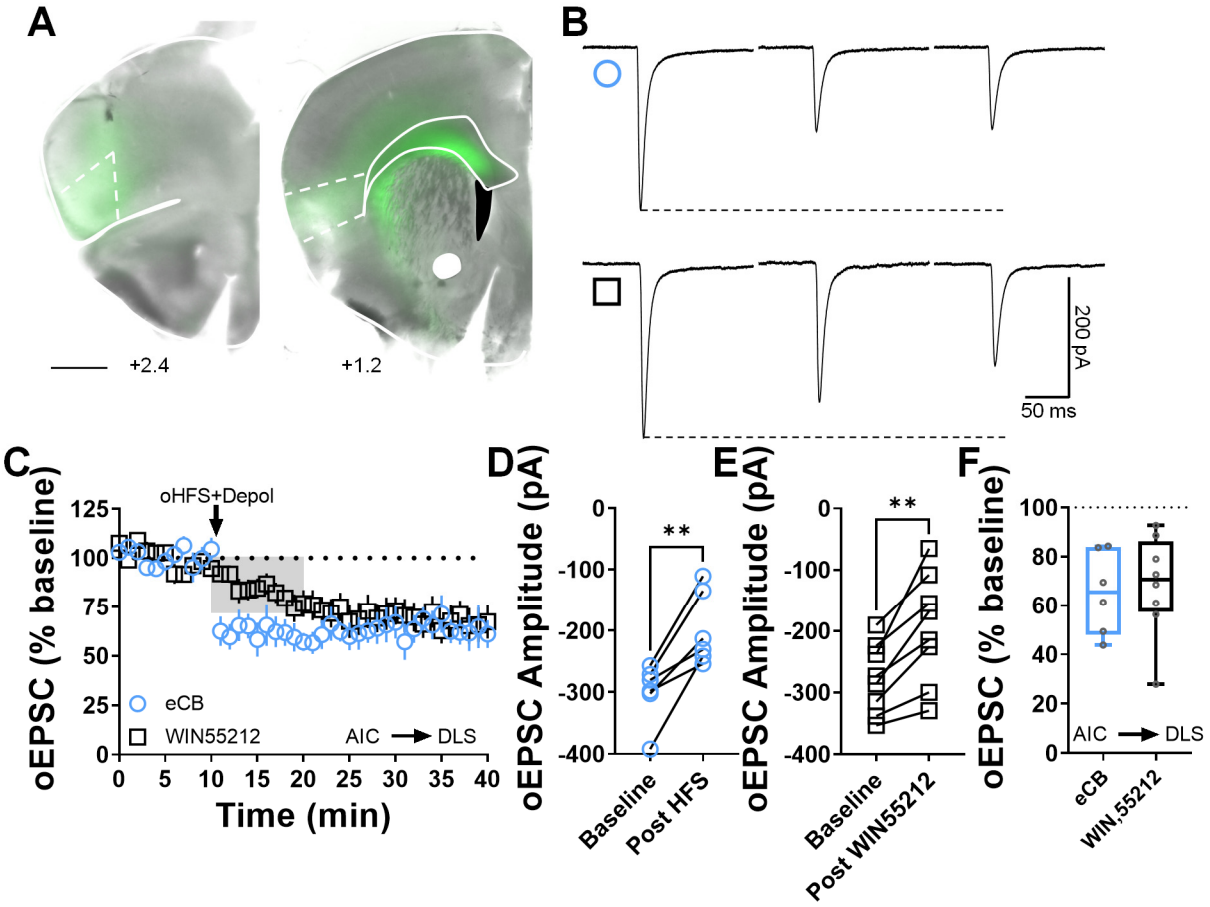

Figure 3. Cannabinoid LTD occurs at AIC-DLS synapses. (A) Coronal brain slice showing the AAV-ChR2 infection of AIC and dorsal striatal terminal expression (bar scale = 1000 µm). **(B)** Representative oEPSC traces showing the effects of pairing optical high frequency stimulation with postsynaptic depolarization (oHFS+Depol, cyan open circle) to induce eCB-LTD and the application of the CB1 agonist, WIN55,212-2 (1 µM, 10 min, black open square) to induce CB1-LTD in brain slices of AAV-ChR2 C57Bl/6J mice. **(C)** Both oHFS and WIN55,212-2 induced AIC-DLS LTD. Data represent mean ± SEM. **(D)** oHFS significantly reduced oEPSC amplitudes (0–10 min baseline v. final 10 min of recording; paired t-test, P = 0.0035, t5=5.2, n = 6 neurons from 4 mice). **(E)** WIN55,212-2 significantly reduced oEPSC amplitudes (0–10 min baseline v. final 10 min of recording; paired t-test, P = 0.0018, t7=4.9, n = 8 neurons from 4 mice). **(F)** The box plot shows the final 10 min of recording average of eCB-(65 ± 7%) and CB1-LTD (68 ± 7%). **P < 0.01.

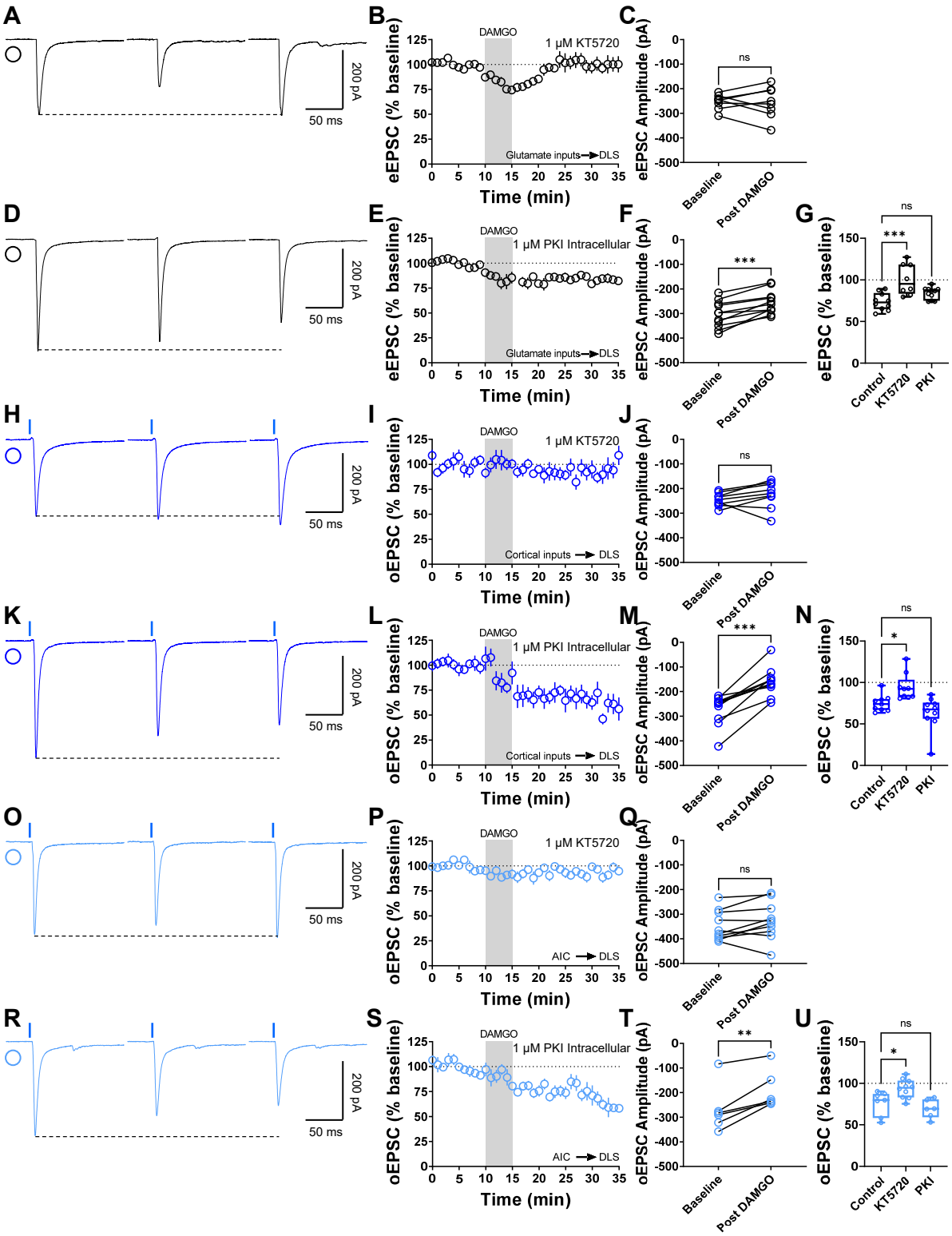

Figure 4. Inhibition of presynaptic PKA blocks MOR-mediated LTD. (A) Representative eEPSC traces showing the effects of DAMGO (0.3 μM, 5 min) application after the preincubation of PKA-selective inhibitor, KT5720 (1 μM, ≥1 hr). **(B-C)** The

preincubation of KT5720 blocked glutamatergic MOR-LTD, the eEPSC amplitudes did not change after DAMGO application (0–10 min baseline v. final 10 min of recording; paired t-test, P = 0.865, t7 =0.176, n = 8 neurons from 3 mice). **(D)** Representative eEPSC traces showing the effects of DAMGO (0.3 μM, 5 min) application after the intracellular dialysis of PKI (1 μM, ≥30 min). **(E-F)** The inhibition of postsynaptic PKA did not alter MOR-LTD. eEPSC amplitudes were reduced after DAMGO application (0–10 min baseline v. final 10 min of recording; paired t-test, P = 0.0001, t10 =6.07, n = 11 neurons from 5 mice). **(G)** Presynaptic PKA inhibition disrupted MOR-LTD (KT5720: 101 ± 7%, P=0.00019 v PKI: 84 ± 2%, P=0.121; F(2,26)=10.65, One-way ANOVA Dunnet's multiple comparison test) **(H)** Representative oEPSC traces showing the effects of DAMGO (0.3 μM, 5 min) application after the preincubation of PKA-selective inhibitor, KT5720 (1 μM, ≥1 hr). **(I-J)** PKA inhibition blocked corticostriatal MOR-LTD, with no changes in oEPSC amplitudes after DAMGO application (0–10 min baseline v. final 10 min of recording; paired t-test, P = 0.183, t8 =1.46, n = 9 neurons from 4 mice). **(K)** Representative oEPSC traces showing the effects of DAMGO (0.3 μM, 5 min) application after the intracellular dialysis of PKI (1 μM, ≥30 min). **(L-M)** The inhibition of postsynaptic PKA did not alter MOR-LTD. oEPSC amplitudes were reduced after DAMGO application (0–10 min baseline v. final 10 min of recording; paired t-test, P = 0.0001, t9 =6.45, n = 10 neurons from 4 mice). **(N)** Presynaptic PKA inhibition disrupted cortical MOR-LTD (KT5720: 94 ± 5%, P=0.0304 v PKI: 64 ± 6%, P=0.24; F(2,25)=8.805, One-way ANOVA Dunnet's multiple comparison test). **(O)** Representative AIC-DLS oEPSC traces showing the effects of DAMGO (0.3 μM, 5 min) application after the preincubation of PKA-selective inhibitor, KT5720 (1 μM, ≥1 hr). **(P-Q)** KT5720 blocked AIC-expressed MOR-LTD, with no changes in oEPSC amplitudes after DAMGO application (0–10 min baseline v. final 10 min of recording; paired t-test, P = 0.141, t9 =1.613, n = 10 neurons from 3 mice). **(R)** Representative AIC-DLS oEPSC traces showing the effects of DAMGO (0.3 μM, 5 min) application after the intracellular dialysis of PKI (1 μM, ≥30 min). **(S-T)** Postsynaptic PKA inhibition did not alter specific AIC MOR-mediated LTD. oEPSC amplitudes were reduced after DAMGO application (0–10 min baseline v. final 10 min of recording; paired t-test, P = 0.0049, t5 =4.8, n = 6 neurons from 3 mice). **(U)** Presynaptic PKA inhibition disrupted AIC MOR-LTD (KT5720: 94 ± 4%, P=0.017 v PKI: 69 ± 5%, P=0.52; F(2,20)=8.411, One-way ANOVA Dunnet's multiple comparison test). Time course data represent mean ± SEM. Box plots show average of the final 10 minutes of recording and represent median and interquartile ranges. ns= not significant, **P < 0.01, ***P < 0.001.

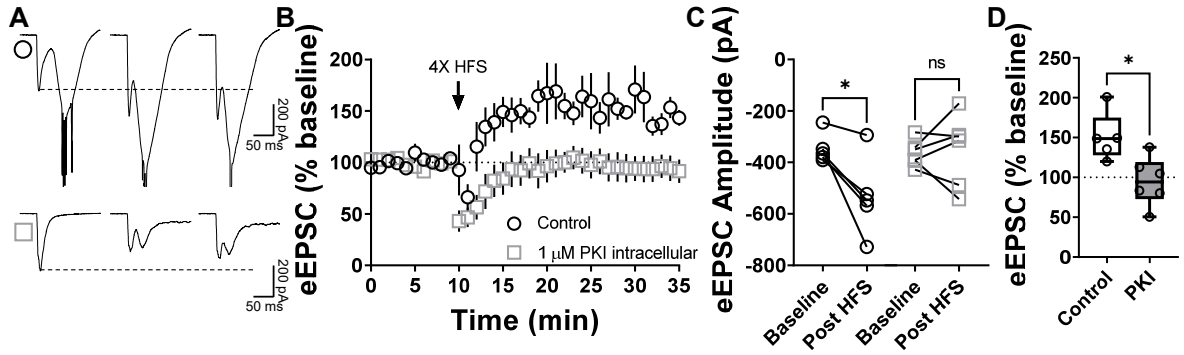

Figure 5. Postsynaptic PKA is required for CA1 hippocampal LTP. (A) Representative eEPSC traces before and after high-frequency stimulation (HFS) (4 pulses of 100 Hz, 1 min inter-pulse interval), showing the effects of PKI (1 μM) intracellular diffusion into MSNs within hippocampal brain slices of C57BL/6J mice. **(B-C)** Post synaptic PKA signaling is necessary to the induction of LTP in CA1 (0–10 min baseline v. final 10 min of recording; Control: paired t-test, $P = 0.03$, $t4 = 3.42$, $n = 5$ neurons from 3 mice; PKI: paired t-test, $P = 0.8$, $t5 = 0.271$, $n = 6$ neurons from 3 mice). **(D)** Box plot shows the average disruption of hippocampal LTP by inhibiting post synaptic PKA (Control: 151 ± 14% vs PKI: 95 ± 12%, $P=0.014$, $t9=3.05$, Unpaired t-test). Time course data represent mean ± SEM. Box plots represent median and interquartile ranges. $^*P < 0.05$.

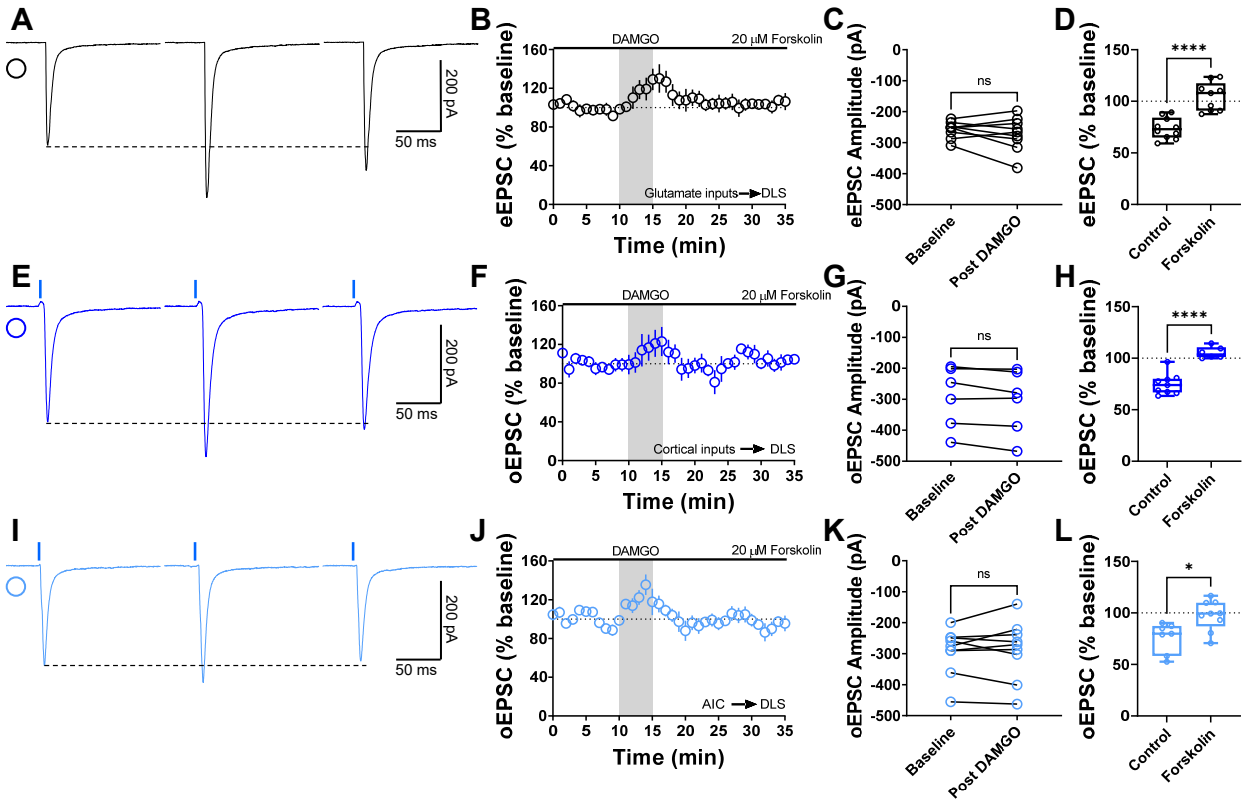

Figure 6. The activation of adenylyl cyclase disrupts MOR-mediated LTD. (A) Representative eEPSC traces showing the effects of 20 μM forskolin before, during and after DAMGO (0.3 μM, 5 min) application. **(B-D)** AC activation disrupted glutamatergic MOR-LTD (105 ± 5%, Unpaired t-test, P=0.00004, t17=5.54), showing no changes in eEPSC amplitude after DAMGO bath application (0–10 min baseline v. final 10 min of recording; paired t-test, P = 0.3236, t8 =1.05, n = 9 neurons from 4 mice). **(E)** Representative oEPSC traces showing the effects of 20 μM forskolin before, during and after DAMGO (0.3 μM, 5 min) application in brain slices from Emx1-Ai32 mice. **(F-H)** AC activation disrupted corticostriatal MOR-LTD (105 ± 2%, Unpaired t-test, P=0.00002, t13=6.65), with no effects in oEPSC amplitude after DAMGO bath application (0–10 min baseline v. final 10 min of recording; paired t-test, P = 0.058, t5 =2.455, n = 6 neurons from 4 mice). **(I)** Representative AIC-DLS oEPSC traces showing the effects of 20 μM forskolin before, during and after DAMGO (0.3 μM, 5 min) application. **(J-L)** AC activation blocked specifically AIC MOR-LTD (98 ± 5%, Unpaired t-test, P=0.012, t14=2.9), without changes in oEPSC amplitude after DAMGO bath application (0–10 min baseline v. final 10 min of recording; paired t-test, P = 0.702, t8 =0.396, n = 9 neurons from 3 mice). Time course data represent mean ± SEM. Box plots show average of the final 10 minutes of recording and represent median and interquartile ranges. ns= not significant.

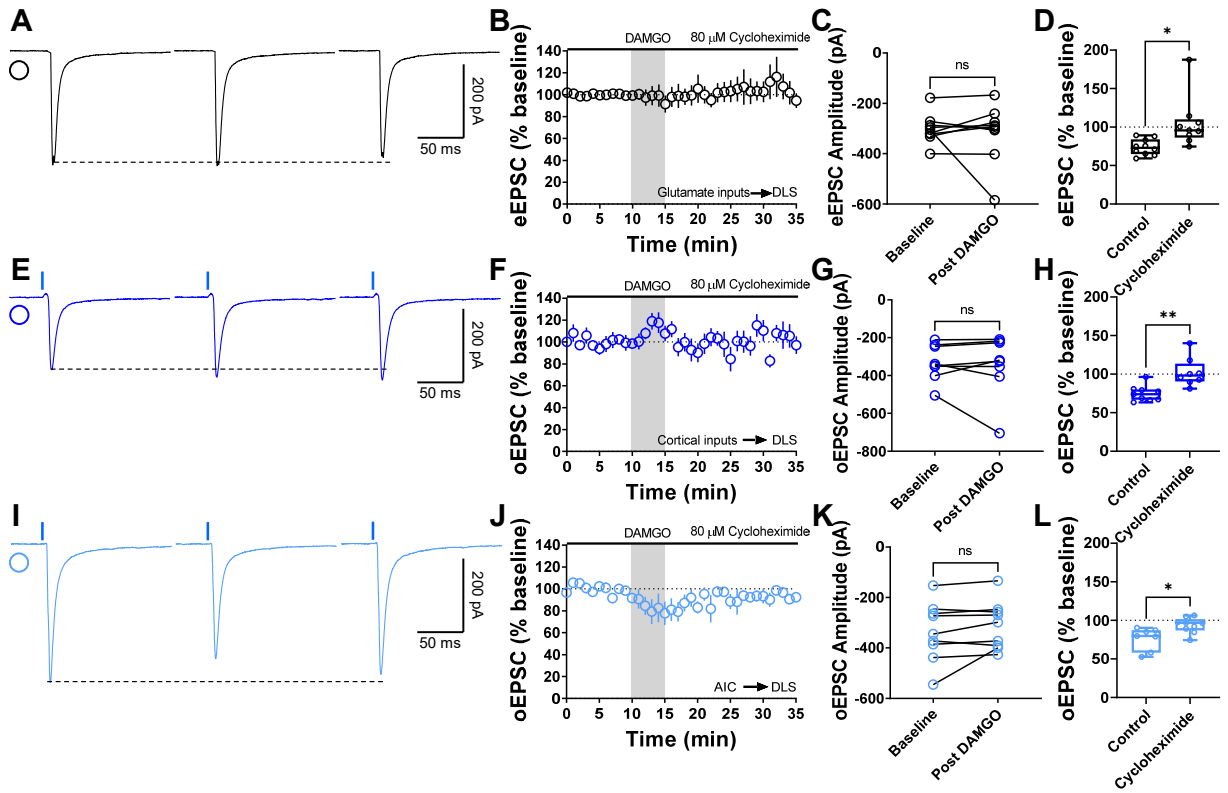

Figure 7. Protein translation is required for MOR-mediated LTD expression. (A) Representative eEPSC traces showing the effects of 80 μM cycloheximide before, during and after DAMGO (0.3 μM, 5 min) application. **(B-D)** Protein translation inhibition disrupted glutamatergic MOR-LTD (105 ± 11%, Unpaired Welch's t-test, P=0.023, t10=2.72), showing no changes in eEPSC amplitude after DAMGO bath application (0–10 min baseline v. final 10 min of recording; paired t-test, P = 0.6506, t8 =0.471, n = 9 neurons from 4 mice). **(E)** Representative oEPSC traces showing the effects of 80 μM cycloheximide before, during and after DAMGO (0.3 μM, 5 min) application in brain slices from Emx1-Ai32 mice. **(F-H)** Protein translation inhibition blocked corticostriatal MOR-LTD (102 ± 7%, Unpaired t-test, P=0.0016, t15=3.83) with no effects in oEPSC amplitude after DAMGO bath application (0–10 min baseline v. final 10 min of recording; paired t-test, P = 0.633, t7 =0.499, n = 8 neurons from 3 mice). **(I)** Representative AIC-DLS oEPSC traces showing the effects of 80 μM cycloheximide before, during and after DAMGO (0.3 μM, 5 min) application. **(J-L)** Protein translation is needed to induce MOR-LTD (94 ± 3%, Unpaired t-test, P=0.013, t14=2.85) from AIC inputs. DAMGO did not change in oEPSC amplitude (0–10 min baseline v. final 10 min of recording; paired t-test, P = 0.163, t8 =1.54, n = 9 neurons from 3 mice). Time course data represent mean ± SEM. Box plots show average of the final 10 minutes of recording and represent median and interquartile ranges. ns= not significant.

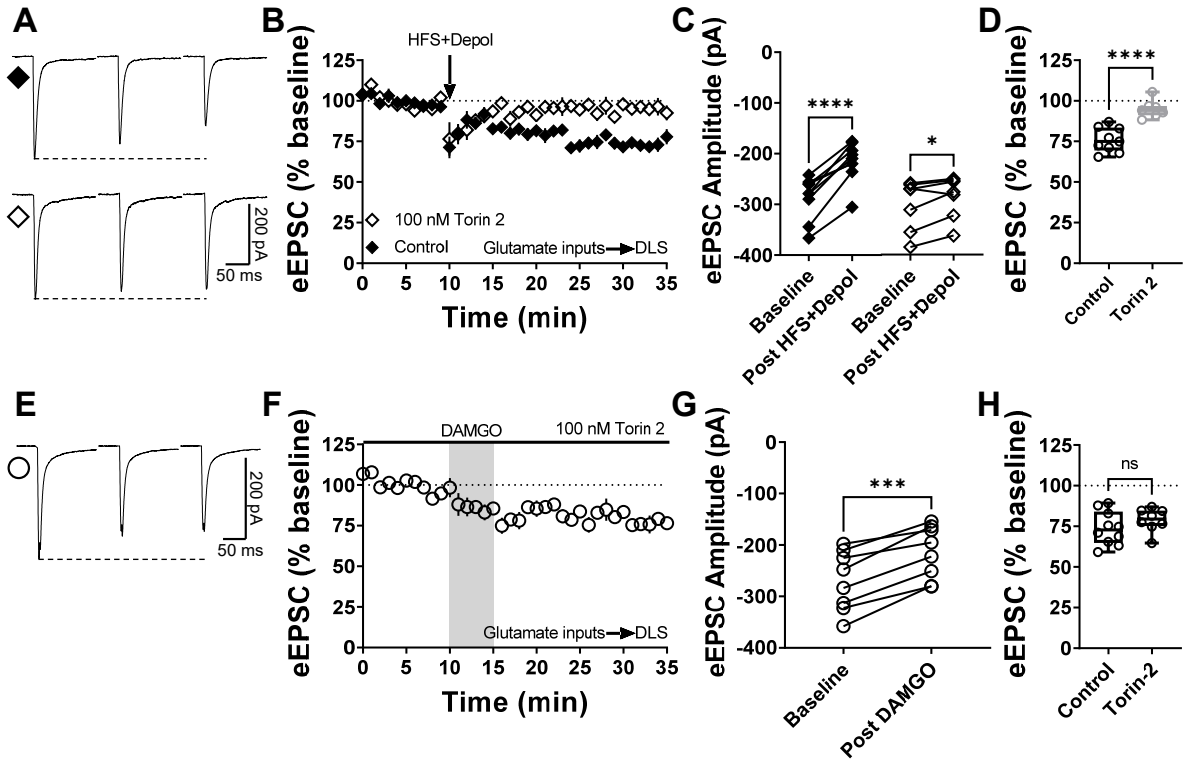

Figure 8. mTOR pathway is involve in eCB-LTD but not in MOR-LTD in the DLS. (A) Representative eEPSC traces before and after high-frequency stimulation (HFS) coupled with depolarization (4 pulses of 100 Hz, 10 s inter-pulse interval), showing the effects of torin 2 (100 nM) bath application in brain slices of C57BL/6J. **(B-C)** mTOR inhibition blocked eCB-LTD in DLS (0–10 min baseline v. final 10 min of recording; Control: paired t-test, P = 0.00003, t8 =8.6, n = 9 neurons from 4 mice; torin 2: paired t-test, P = 0.04, t6 =2.62, n = 7 neurons from 3 mice). **(D)** Torin 2 disrupted eCB-LTD in the DLS (control: 76 ± 3% vs torin 2: 95 ± 2, Unpaired t-test, P=0.00006, t14=5.64) **(E)** Representative eEPSC traces before and after DAMGO bath application (0.3 µM, 5 min), showing the effects of torin 2 (100 nM) bath application in brain slices of C57BL/J. **(F-G)** mTOR inhibition did not affect the expression of MOR-LTD in DLS (0–10 min baseline v. final 10 min of recording; paired t-test, P = 0.0001, t7 =7.48, n = 8 neurons from 3 mice). **(H)** Torin 2 did not blocked MOR-LTD in the DLS (control: 74 ± 3% vs torin 2: 79 ± 3, Unpaired t-test, P=0.25, t16=1.19). Time course data represent mean ± SEM. Box plots show average of the final 10 minutes of recording and represent median and interquartile ranges. ns = not significant, ***P < 0.001, ****P < 0.0001.

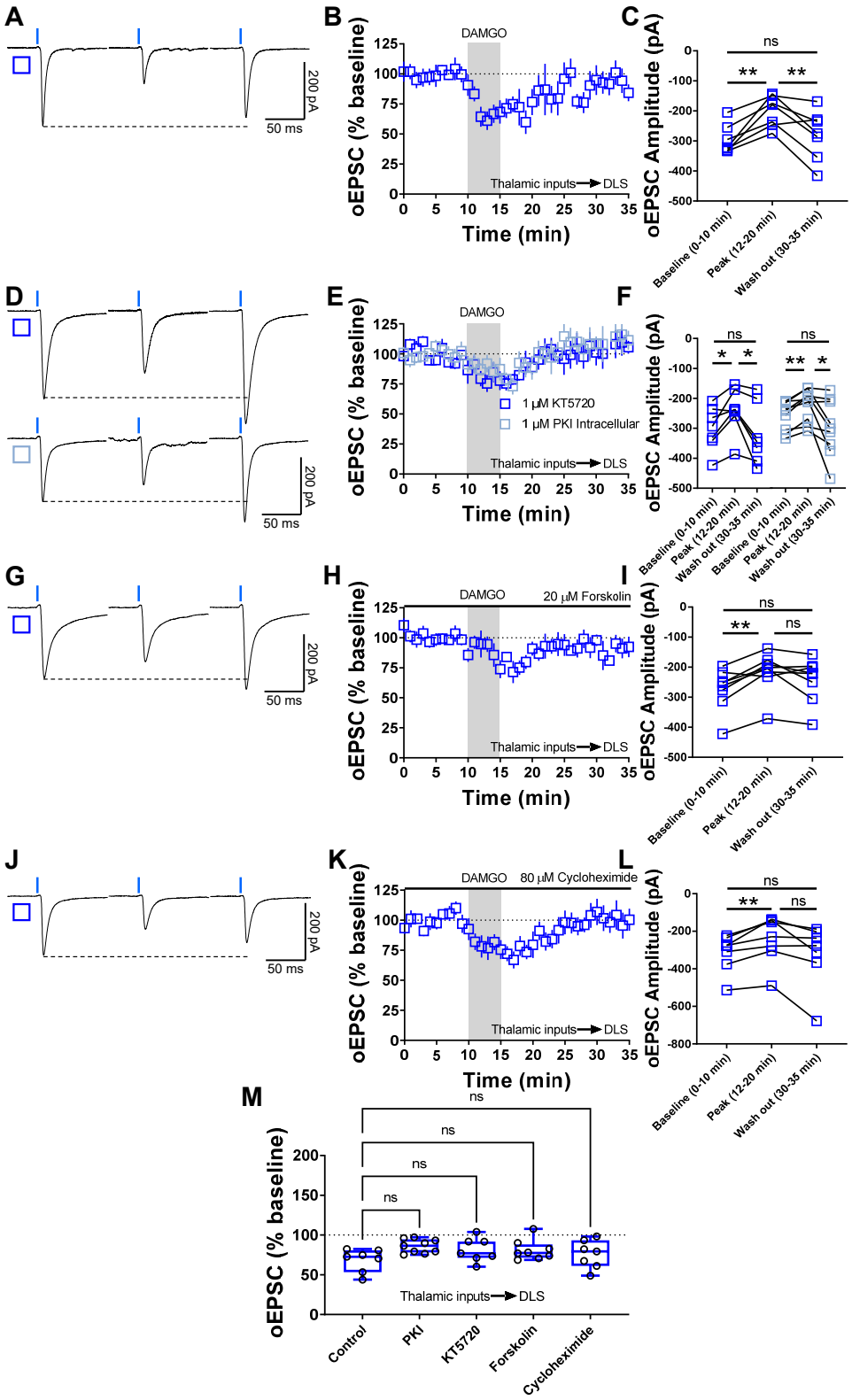

686

687 **Figure 9. MOR-STD is not affected by PKA inhibition, cAMP activation or protein**
688 **translation inhibition. (A)** Representative optically-evoked EPSC traces before, during

and after DAMGO (0.3 μM, 5 min) application in brain slices from VGluT2-Ai32 mice. **(B-C)** Thalamocortical inputs produced MOR-STD in DLS from VGluT2-Ai32 mice (10 min baseline v. peak 12-20 min of recording P=0.0027; 12-20 min Peak v 30-35 min Wash out of recording, P=0.089, Repeated measure One-way ANOVA Tukey's test, n = 7 neurons from 3 mice). **(D)** Representative oEPSC traces showing the effects of DAMGO (0.3 μM, 5 min) application after the preincubation of PKA-selective inhibitor KT5720 (1 μM, ≥1 hr, blue open square) and after the intracellular dialysis of PKI (1 μM, ≥30 min, cyan open square). **(E-F)** The inhibition of pre (1 μM KT5720) and postsynaptic PKA (1 μM PKI) did not affected MOR-STD (KT5720: 10 min baseline v. peak 12-20 min of recording , P=0.035; 12-20 min Peak v 30-35 min Wash out of recording, P = 0.035, Repeated measure One-way ANOVA Tukey's test, n = 7 neurons from 3 mice) (PKI:, 10 min baseline v. peak 12-20 min of recording, P = 0.0022; 12-20 min Peak v 30-35 min Wash out of recording , P=0.043, Repeated measure One-way ANOVA Tukey's test, n = 9 neurons from 3 mice). **(G)** Representative oEPSC traces showing the effects of 20 μM forskolin before, during and after DAMGO (0.3 μM, 5 min) application in brain slices from VGluT2-Ai32 mice. **(H-I)** MOR-STD was unaffected after the activation of AC by 20 μM forskolin (10 min baseline v. peak 12-20 min of recording, P=0.0026;12-20 min Peak v 30-35 min Wash out of recording, P=0.168, Repeated measure One-way ANOVA Tukey's test, n = 8 neurons from 4 mice)**. (J)** Representative oEPSC traces showing the effects of 80 μM cycloheximide before, during and after DAMGO (0.3 μM, 5 min) application in brain slices from VGluT2-Ai32 mice. **(K-L)** Protein translation is not necessary for the expression of MOR-STD (10 min baseline v. peak 12-20 min of recording, P=0.0097;12-20 min Peak v 30-35 min Wash out of recording, P=0.082, Repeated measure One-way ANOVA Tukey's test, n = 7 neurons from 3 mice). **(M)** The box plot illustrates the average peak current (12-20 min) and summarize the findings on MOR-STD mechanism in the DLS (One-way ANOVA Dunnett's multiple comparisons test). Time course data represent mean ± SEM. Box plots represent median and interquartile ranges and show average peak responses (12-20 minutes). ns=not significant, *P < 0.05, **P < 0.01.

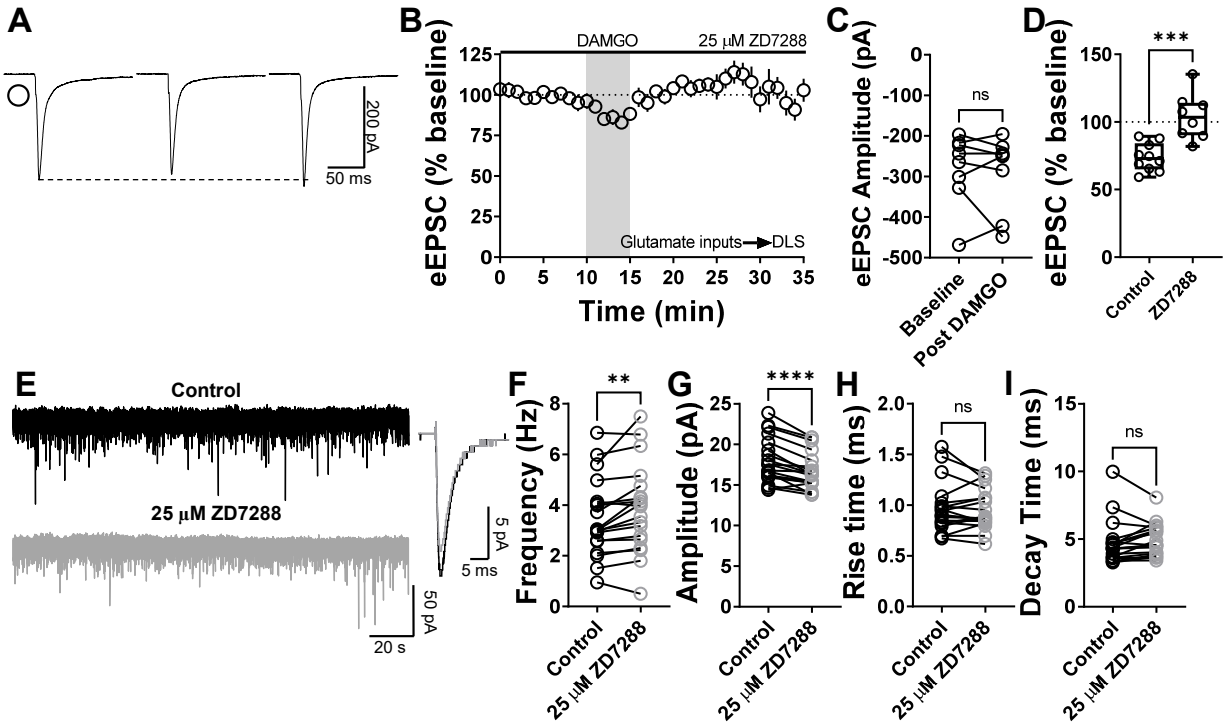

Figure 10. Inhibition of striatal HCN channels disrupts MOR-mediated LTD. (A) Representative eEPSC traces showing the effects of 25 μM ZD7288 before, during and after DAMGO (0.3 μM, 5 min) application. **(B-D)** HCN channel inhibition disrupted glutamatergic MOR-LTD (104 ± 6%, Unpaired t-test, P=0.0003, t16=4.67) in the DLS, showing no changes in eEPSC amplitude after DAMGO bath application (0–10 min baseline v. final 10 min of recording; paired t-test, P = 0.64, t7 =0.496, n = 8 neurons from 4 mice). **(E)** Representative synaptic current traces from C57BL/6J mice showing the spontaneous excitatory postsynaptic currents (sEPSC) in absence (black trace) or presence of 25 μM ZD7288 (gray trace, 15 min) application. **(F-I)** HCN channel inhibition increased frequency (paired t-test, P = 0.006, t18 =3.113, n = 19 neurons from 3 mice) and decreased amplitude (paired t-test, P = 0.00002, t18 =5.88, n = 19 neurons from 3 mice), without changes in rise (paired t-test, P = 0.61, t18 =0.522, n = 19 neurons from 3 mice) and decay times (paired t-test, P = 0.21, t18 =1.314, n = 19 neurons from 3 mice) of the sEPSC events in DLS. Time course data represent mean ± SEM. Box plots show average of the final 10 minutes of recording and represent median and interquartile ranges. ns= not significant, **P < 0.001, ****P < 0.0001.

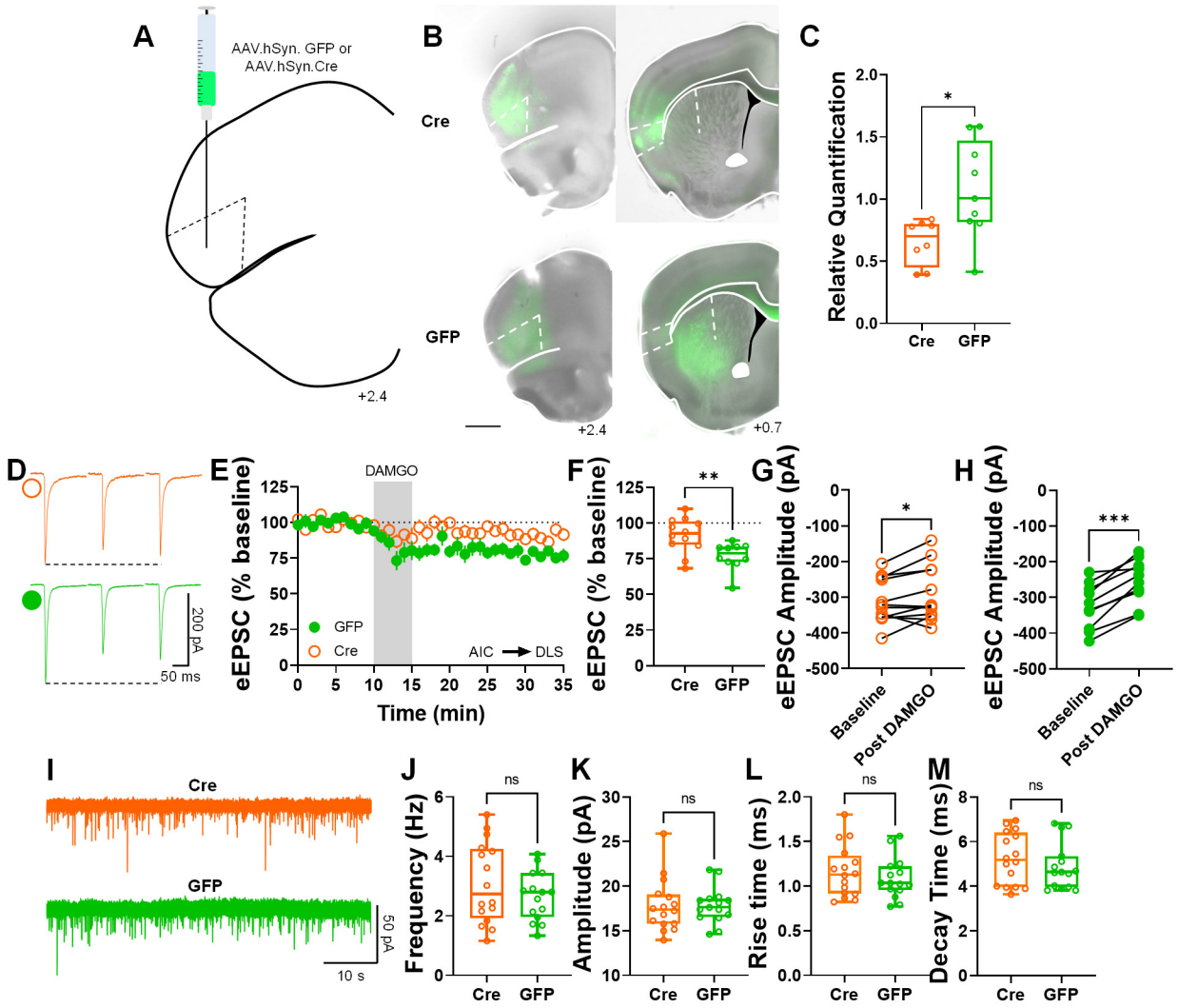

Figure 11. Genetic ablation of HCN1 channels in the AIC reduce MOR-mediated LTD expression in the DLS. (A) Schematic figure of coronal brain slice showing injection paradigm enabling knock out of HCN1 channel expression in AIC in HCN1-flox mice. An AAV vector encoding for either cre-recombinase (AAV.hSyn.cre) or eGFP (AAV.hSyn.eGFP) was injected at least 4 weeks prior to recordings. **(B)** Coronal brain slice showing the AAV-cre or AAV-GFP infection of AIC and dorsal striatal terminal expression (bar scale = 1000 µm). **(C)** AAV.cre reduced the expression of HCN1 in the AIC after 4 weeks post injection (cre: 0.65 ± 0.06 vs GFP: 1.07 ± 0.13). **(D)** Representative eEPSC traces showing the effects of DAMGO (0.3 µM, 5 min) application in brain slices of AAV-injected HCN1-flox mice. **(E-F)** The conditional decrease of HCN1 channel from AIC, blunted MOR-LTD in DLS (cre: 91 ± 4% vs GFP: 77 ± 3%, Unpaired t-test, P=0.0063, t20=3.05, n=12 neurons from 6 cre-injected mice and n=10 neurons from 4 GFP-injected mice). **(G)** HCN1 reduction did not fully disrupt MOR-LTD, because there was still a small, but significant reduction of eEPSC amplitude after DAMGO application (0–10 min baseline v. final 10 min of recording; paired t-test, P = 0.042, t11 =2.31, n = 12 neurons from 6 mice). **(H)** Control GFP-injected mice showed normal decrease of eEPSC

amplitude after DAMGO application 0–10 min baseline v. final 10 min of recording; paired t-test, $P = 0.0001$, $t_9 = 6.55$, $n = 10$ neurons from 4 mice). **(I)** Representative synaptic current traces from HCN1-flox mice showing the spontaneous excitatory postsynaptic currents (sEPSCs) in AAV-cre (orange trace) and AAV-GFP (green trace) injected mice. **(J-M)** HCN1 channel ablation from AIC synapses did not affect frequency (cre: 3.1 ± 0.3 Hz vs GFP: 2.7 ± 0.2 Hz, Unpaired t-test, P=0.28, t29=1.11, n=16 neurons from 4 cre-injected mice and n=15 neurons from 3 GFP-injected mice), amplitude (cre: 17.8 ± 0.7 pA vs GFP: 17.8 ± 0.5 pA, Unpaired t-test, P=0.98, t29=0.025, n=16 neurons from 4 cre-injected mice and n=15 neurons from 3 GFP-injected mice), rise time (cre: 1.16 ± 0.07 ms vs GFP: 1.09 ± 0.06 ms, Unpaired t-test, P=0.42, t29=0.822, n=16 neurons from 4 cre-injected mice and n=15 neurons from 3 GFP-injected mice) and decay time (cre: 5.24 ± 0.29 ms vs GFP: 4.9 ± 0.27 ms, Unpaired t-test, P=0.4, t29=0.396, n=16 neurons from 4 cre-injected mice and n=15 neurons from 3 GFP-injected mice) of the sEPSC events in DLS. Time course data represent mean ± SEM. Box plots show average of the final 10 minutes of recording and represent median and interquartile ranges. ns= not significant, *P < 0.05, **P < 0.01, ***P < 0.001.

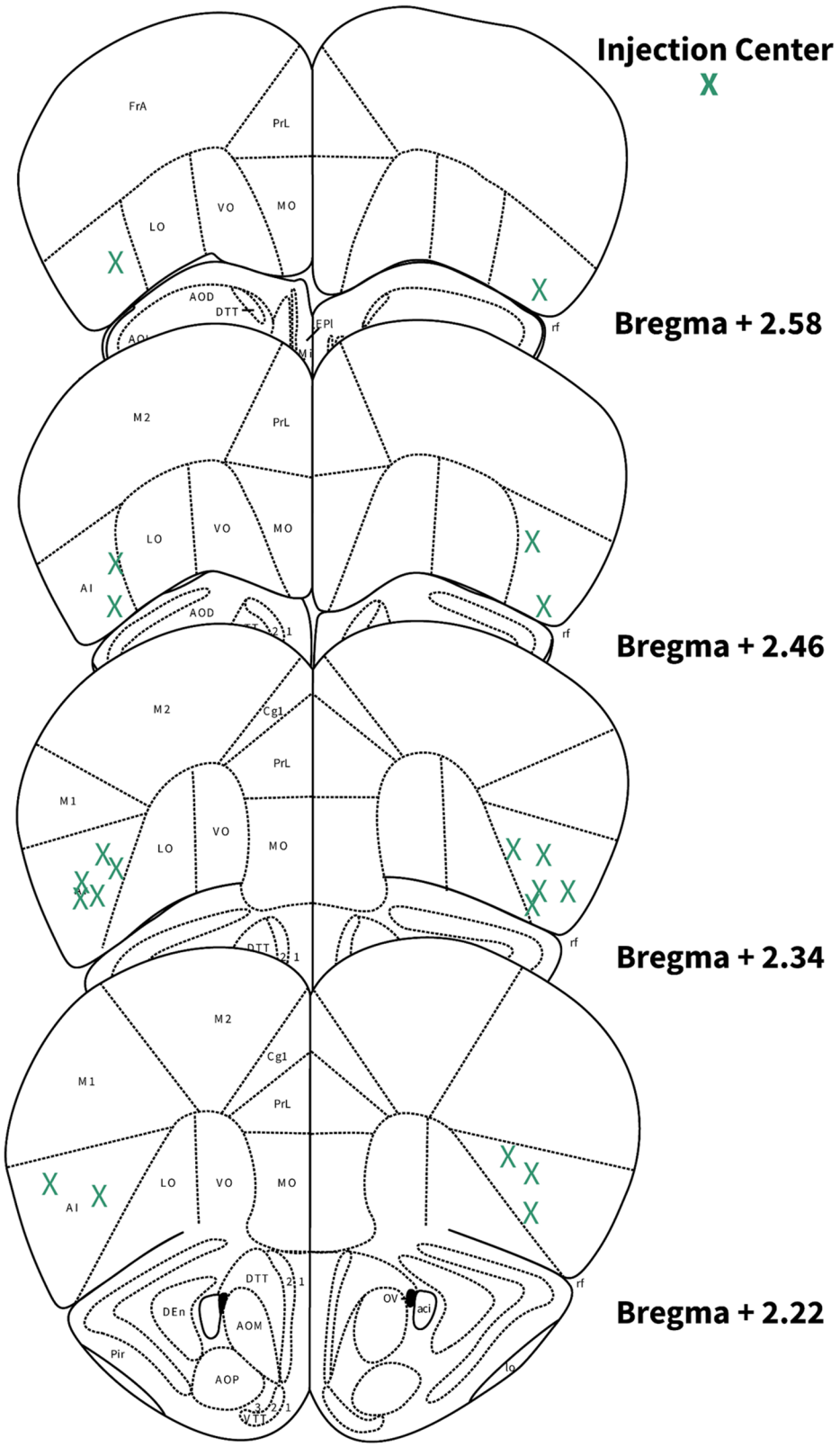
Injection Center
X
FrA
PrL
LO
VO
MO
AOD
DTT
EPl
rf
Bregma + 2.58
M2
PrL
LO
VO
MO
AI
AOD
rf
Bregma + 2.46
M2
Cg1
PrL
M1
LO
VO
MO
rf
Bregma + 2.34
M2
Cg1
M1
PrL
AI
LO
VO
MO
DTT
DEn
AOM
OV
aci
Pir
AOP
VTT
rf
Bregma + 2.22

771 **Figure 12. Locations of AIC injections for DLS electrophysiology.** Schematic images
772 of coronal brain slices modified from Allen Mouse Brain Atlas showing the bilateral
773 injection centers of AAV-cre and EGFP in the AIC of HCN1-flox mice as verified by
774 histology.

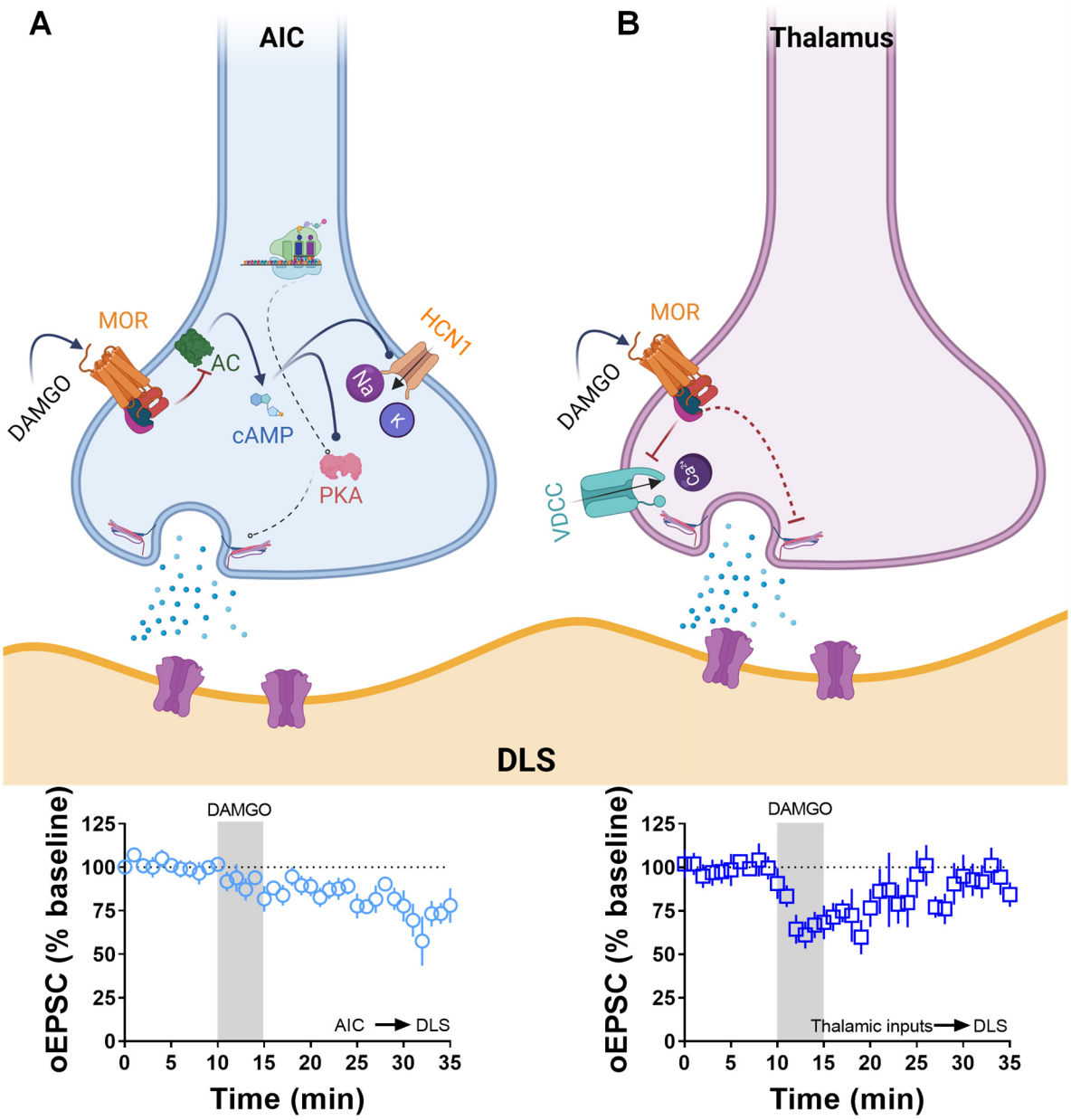

Figure 13. Summary of the proposed presynaptic signaling pathways that are involved in MOR-mediated LTD and STD. (A) The activation of MOR at AIC inputs in the DLS induces a decrease in the production of cAMP (via adenylyl cyclase (AC) inhibition), which impacts the activation of HCN1 channels and the function of presynaptic PKA. Furthermore, the presence of local protein synthesis is critical for the maintaining of the glutamatergic LTD shown below. **(B)** The activation of MOR at thalamic inputs in the DLS does not utilize the mechanisms illustrated in **(A)**. Therefore, the mechanism is conceptualized to involve MOR-driven Gβγ block of voltage dependent calcium channels (VDCC) producing a transitory reduction in the release of glutamate in the DLS as shown below. Schematic figure was created with BioRender.com.

786 ## References

787 Asih PR, Prikas E, Stefanoska K, Tan ARP, Ahel HI & Ittner A. (2020). Functions of p38 MAP Kinases in the
788 Central Nervous System. *Frontiers in Molecular Neuroscience* **13**.

789
790 Atwood BK, Kupferschmidt DA & Lovinger DM. (2014a). Opioids induce dissociable forms of long-term
791 depression of excitatory inputs to the dorsal striatum. *Nat Neurosci* **17,** 540-548.

792
793 Atwood BK, Lovinger DM & Mathur BN. (2014b). Presynaptic long-term depression mediated by Gi/o-
794 coupled receptors. *Trends Neurosci* **37,** 663-673.

795
796 Bao G, Kang L, Li H, Li Y, Pu L, Xia P, Ma L & Pei G. (2007). Morphine and heroin differentially modulate in
797 vivo hippocampal LTP in opiate-dependent rat. *Neuropsychopharmacology* **32,** 1738-1749.

798
799 Boyes J, Bolam JP, Shigemoto R & Stanford IM. (2007). Functional presynaptic HCN channels in the rat
800 globus pallidus. *European Journal of Neuroscience* **25,** 2081-2092.

801
802 Burton AC, Nakamura K & Roesch MR. (2015). From ventral-medial to dorsal-lateral striatum: neural
803 correlates of reward-guided decision-making. *Neurobiol Learn Mem* **117,** 51-59.

804
805 Chen I & Lui F. (2021). Neuroanatomy, Neuron Action Potential. In *StatPearls*. StatPearls Publishing

806 Copyright © 2021, StatPearls Publishing LLC., Treasure Island (FL).

807
808 Cho HS, Lee HH, Choi SJ, Kim KJ, Jeun SH, Li Q-Z & Sung K-W. (2008). Forskolin Enhances Synaptic
809 Transmission in Rat Dorsal Striatum through NMDA Receptors and PKA in Different Phases. *kjpp*
810 **12,** 293-297.

811
812 Corbit LH & Janak PH. (2016). Habitual Alcohol Seeking: Neural Bases and Possible Relations to Alcohol
813 Use Disorders. *Alcoholism: Clinical and Experimental Research* **40,** 1380-1389.

814
815 Dacher M & Nugent FS. (2011a). Morphine-induced modulation of LTD at GABAergic synapses in the
816 ventral tegmental area. *Neuropharmacology* **61,** 1166-1171.

817
818 Dacher M & Nugent FS. (2011b). Opiates and plasticity. *Neuropharmacology* **61,** 1088-1096.

819
820 DePoy L, Daut R, Brigman JL, MacPherson K, Crowley N, Gunduz-Cinar O, Pickens CL, Cinar R, Saksida LM,
821 Kunos G, Lovinger DM, Bussey TJ, Camp MC & Holmes A. (2013). Chronic alcohol produces
822 neuroadaptations to prime dorsal striatal learning. *Proc Natl Acad Sci U S A* **110,** 14783-14788.

823

824 Drake CT, Chavkin C & Milner TA. (2007). Opioid systems in the dentate gyrus. *Prog Brain Res* **163,** 245-
825 263.

826

827 Duffy SN & Nguyen PV. (2003). Postsynaptic Application of a Peptide Inhibitor of cAMP-Dependent Protein
828 Kinase Blocks Expression of Long-Lasting Synaptic Potentiation in Hippocampal Neurons. *The*
829 *Journal of Neuroscience* **23,** 1142-1150.

830

831 Everitt BJ & Robbins TW. (2016). Drug Addiction: Updating Actions to Habits to Compulsions Ten Years
832 On. *Annual Review of Psychology* **67,** 23-50.

833

834 Fritz BM, Munoz B & Atwood BK. (2019). Genetic Selection for Alcohol Preference in Mice Alters Dorsal
835 Striatum Neurotransmission. *Alcohol Clin Exp Res* **43,** 2312-2321.

836

837 Fritz BM, Munoz B, Yin F, Bauchle C & Atwood BK. (2018). A High-fat, High-sugar 'Western' Diet Alters
838 Dorsal Striatal Glutamate, Opioid, and Dopamine Transmission in Mice. *Neuroscience* **372,** 1-15.

839

840 Gremel CM, Chancey JH, Atwood BK, Luo G, Neve R, Ramakrishnan C, Deisseroth K, Lovinger DM & Costa
841 RM. (2016). Endocannabinoid Modulation of Orbitostriatal Circuits Gates Habit Formation.
842 *Neuron* **90,** 1312-1324.

843

844 Hawes SL, Salinas AG, Lovinger DM & Blackwell KT. (2017). Long-term plasticity of corticostriatal synapses
845 is modulated by pathway-specific co-release of opioids through κ-opioid receptors. *J Physiol* **595,**
846 5637-5652.

847

848 He C, Chen F, Li B & Hu Z. (2014). Neurophysiology of HCN channels: from cellular functions to multiple
849 regulations. *Prog Neurobiol* **112,** 1-23.

850

851 Hilário MRF & Costa RM. (2008). High on habits. *Front Neurosci* **2,** 208-217.

852

853 Hopf FW & Lesscher HMB. (2014). Rodent models for compulsive alcohol intake. *Alcohol* **48,** 253-264.

854

855 Huang Z, Li G, Aguado C, Lujan R & Shah MM. (2017). HCN1 channels reduce the rate of exocytosis from a
856 subset of cortical synaptic terminals. *Sci Rep* **7,** 40257.

857

858 Huang Z, Lujan R, Kadurin I, Uebele VN, Renger JJ, Dolphin AC & Shah MM. (2011). Presynaptic HCN1
859 channels regulate CaV3.2 activity and neurotransmission at select cortical synapses. *Nature*
860 *Neuroscience* **14,** 478-486.

861

862 Iremonger KJ & Bains JS. (2009). Retrograde opioid signaling regulates glutamatergic transmission in the
863 hypothalamus. *J Neurosci* **29,** 7349-7358.

Le Merrer J, Becker JAJ, Befort K & Kieffer BL. (2009). Reward processing by the opioid system in the brain. *Physiol Rev* **89,** 1379-1412.

Lockhead S, Moskaleva A, Kamenz J, Chen Y, Kang M, Reddy AR, Santos SDM & Ferrell JE, Jr. (2020). The Apparent Requirement for Protein Synthesis during G2 Phase Is due to Checkpoint Activation. *Cell Rep* **32,** 107901.

Lonart G, Schoch S, Kaeser PS, Larkin CJ, Südhof TC & Linden DJ. (2003). Phosphorylation of RIM1alpha by PKA triggers presynaptic long-term potentiation at cerebellar parallel fiber synapses. *Cell* **115,** 49-60.

Lovinger DM. (2010). Neurotransmitter roles in synaptic modulation, plasticity and learning in the dorsal striatum. *Neuropharmacology* **58,** 951-961.

Mato S, Lafourcade M, Robbe D, Bakiri Y & Manzoni OJ. (2008). Role of the cyclic-AMP/PKA cascade and of P/Q-type Ca++ channels in endocannabinoid-mediated long-term depression in the nucleus accumbens. *Neuropharmacology* **54,** 87-94.

Moosmang S, Biel M, Hofmann F & Ludwig A. (1999). Differential distribution of four hyperpolarization-activated cation channels in mouse brain. *Biol Chem* **380,** 975-980.

Munoz B, Fritz BM, Yin F & Atwood BK. (2018). Alcohol exposure disrupts mu opioid receptor-mediated long-term depression at insular cortex inputs to dorsolateral striatum. *Nat Commun* **9,** 1318.

Muñoz B, Haggerty DL & Atwood BK. (2020). Synapse-specific expression of mu opioid receptor long-term depression in the dorsomedial striatum. *Scientific Reports* **10,** 7234.

Nazzaro C, Greco B, Cerovic M, Baxter P, Rubino T, Trusel M, Parolaro D, Tkatch T, Benfenati F, Pedarzani P & Tonini R. (2012). SK channel modulation rescues striatal plasticity and control over habit in cannabinoid tolerance. *Nat Neurosci* **15,** 284-293.

O'Tousa D & Grahame N. (2014). Habit formation: Implications for alcoholism research. *Alcohol* **48,** 327-335.

Patton MH, Roberts BM, Lovinger DM & Mathur BN. (2016). Ethanol Disinhibits Dorsolateral Striatal Medium Spiny Neurons Through Activation of A Presynaptic Delta Opioid Receptor. *Neuropsychopharmacology* **41,** 1831-1840.

Postea O & Biel M. (2011). Exploring HCN channels as novel drug targets. *Nat Rev Drug Discov* **10,** 903-914.

905
906 Reeves KC, Shah N, Muñoz B & Atwood BK. (2022). Opioid Receptor-Mediated Regulation of
907 Neurotransmission in the Brain. *Frontiers in Molecular Neuroscience* **15**.

908
909 Renteria R, Cazares C & Gremel CM. (2020). Habitual Ethanol Seeking and Licking Microstructure of
910 Enhanced Ethanol Self-Administration in Ethanol-Dependent Mice. *Alcohol Clin Exp Res* **44,** 880-
911 891.

912
913 Salling MC & Harrison NL. (2020). Constitutive Genetic Deletion of Hcn1 Increases Alcohol Preference
914 during Adolescence. *Brain Sci* **10**.

915
916 Sartiani L, Mannaioni G, Masi A, Novella Romanelli M & Cerbai E. (2017). The Hyperpolarization-Activated
917 Cyclic Nucleotide–Gated Channels: from Biophysics to Pharmacology of a Unique Family of Ion
918 Channels. *Pharmacological Reviews* **69,** 354-395.

919
920 Shen F, Jin S, Duan Y, Liang J, Zhang M, Jiang F & Sui N. (2018). Distinctive Changes of L-Type Calcium
921 Channels and Dopamine Receptors in the Dorsomedial and Dorsolateral Striatum after the
922 Expression of Habitual Cocaine-Seeking Behavior in Rats. *Neuroscience* **370,** 139-147.

923
924 Wu YW, Kim JI, Tawfik VL, Lalchandani RR, Scherrer G & Ding JB. (2015). Input- and cell-type-specific
925 endocannabinoid-dependent LTD in the striatum. *Cell Rep* **10,** 75-87.

926
927 Yasuda H, Huang Y & Tsumoto T. (2008). Regulation of excitability and plasticity by endocannabinoids and
928 PKA in developing hippocampus. *Proceedings of the National Academy of Sciences* **105,** 3106-
929 3111.

930
931 Yin HH, Davis MI, Ronesi JA & Lovinger DM. (2006). The Role of Protein Synthesis in Striatal Long-Term
932 Depression. *The Journal of Neuroscience* **26,** 11811-11820.

933
934 Younts TJ, Monday HR, Dudok B, Klein ME, Jordan BA, Katona I & Castillo PE. (2016). Presynaptic Protein
935 Synthesis Is Required for Long-Term Plasticity of GABA Release. *Neuron* **92,** 479-492.

936

937